Signatures of sub-solar mass Primordial Black Holes

Po-Yan Tseng (NTHU)

Collaborators:
Danny Marfatia (*U. of Hawaii*),
Jan Tristram Acuna(NTHU),
Pin-Jung Chen(NTHU),
Yu-Min Yeh(NTHU),

References:
2305.14399, 2304.10084, 2212.13035, 2209.01552

The 3rd International Joint Workshop on the Standard Model and Beyond
and the 11th KIAS Workshop on Particle Physics and Cosmology

DM candidate

- Range of DM mass:

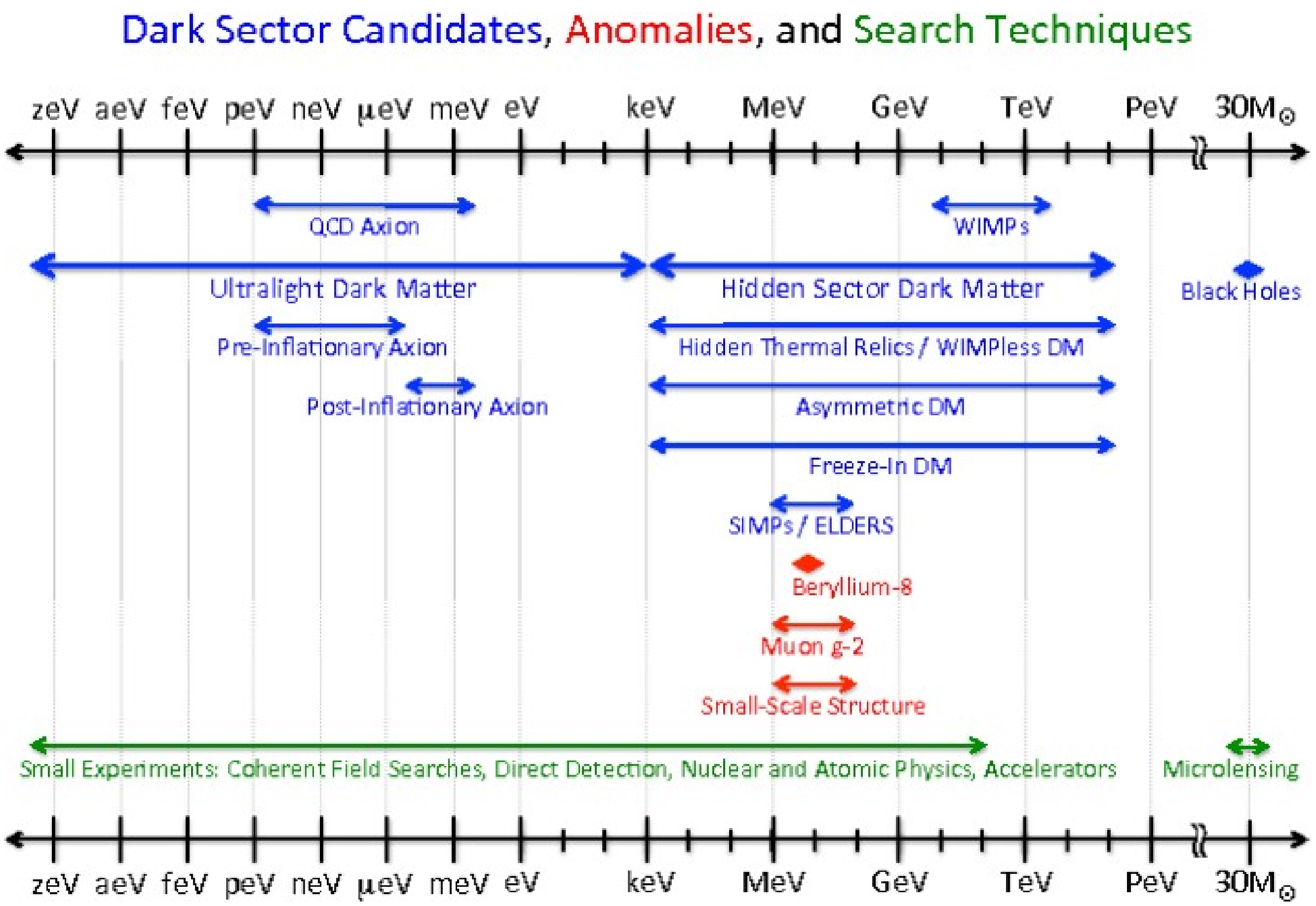

CERN document Server: US:Cosmic Visions: New ideas in dark matter 2017

DM candidate

- Range of DM mass:

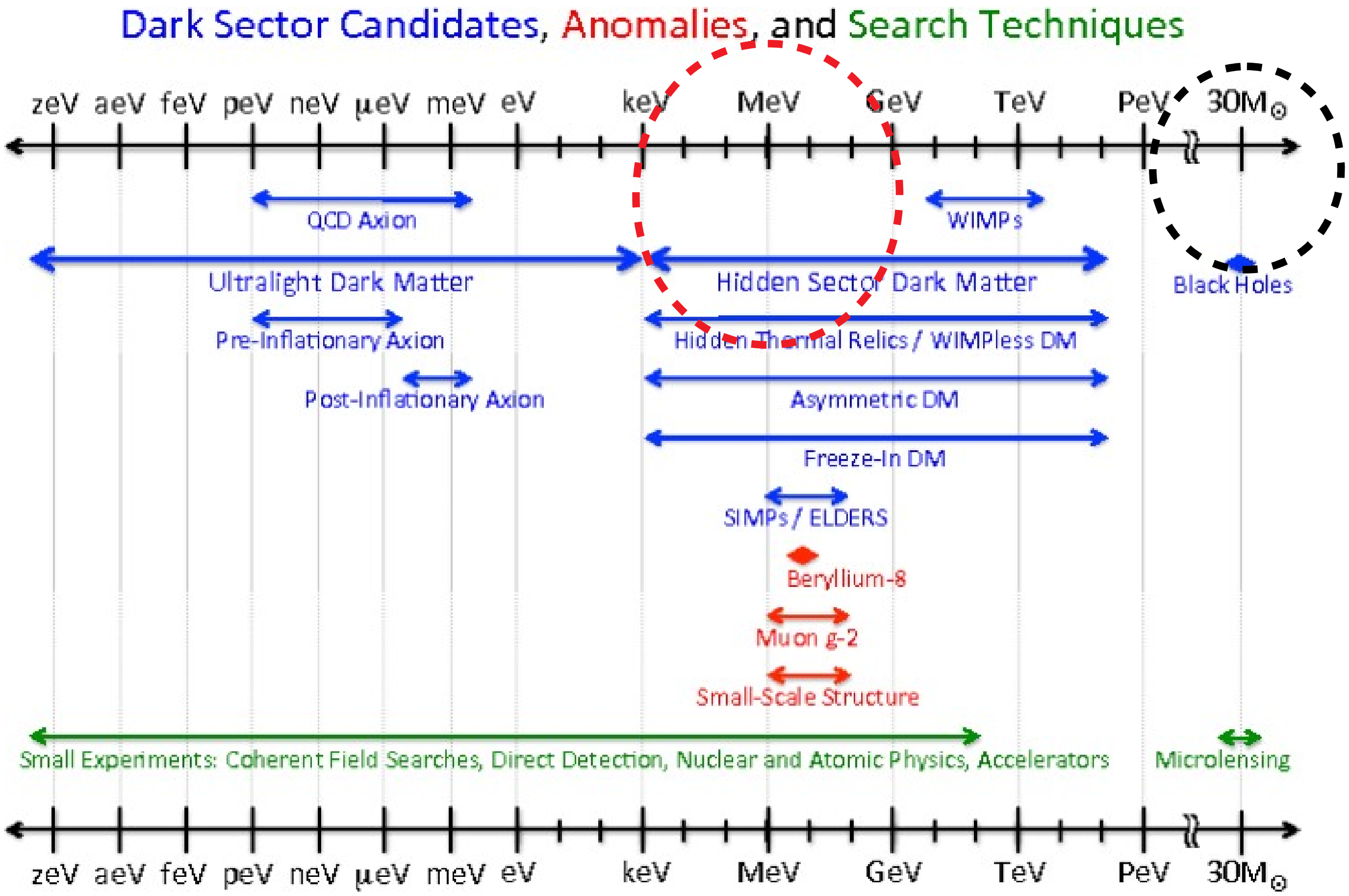

CERN document Server: US:Cosmic Visions: New ideas in dark matter 2017

PBH constraints

- Mass range of PBH (Primordial Black Holes):

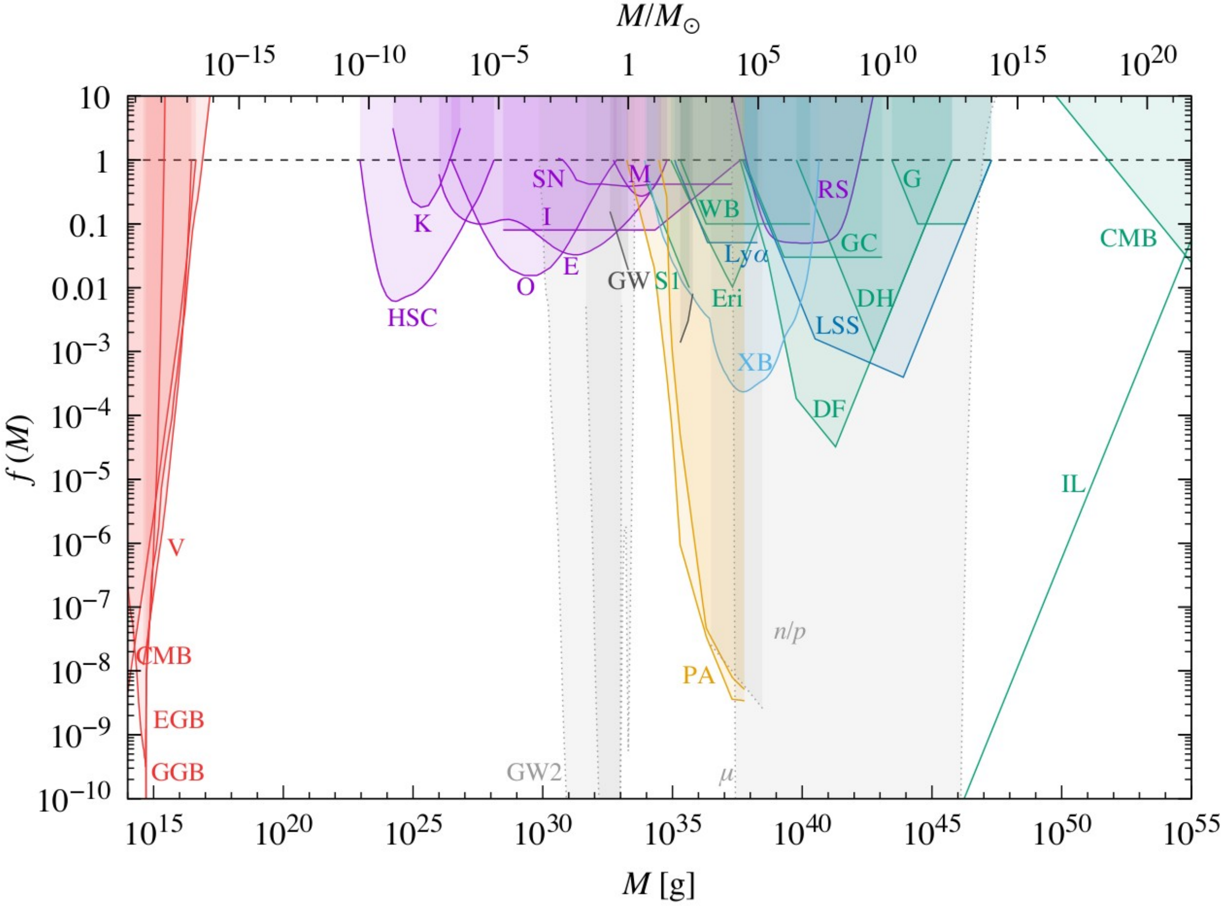

B.Carr, K.Kohri, Y.Sendouda, and J.Yokoyama, arXiv:2002.12778

PBH constraints

- Bounds on the PBH fraction:

B.Carr, K.Kohri,Y.Sendouda,J.Yokoyama: 2002.12778

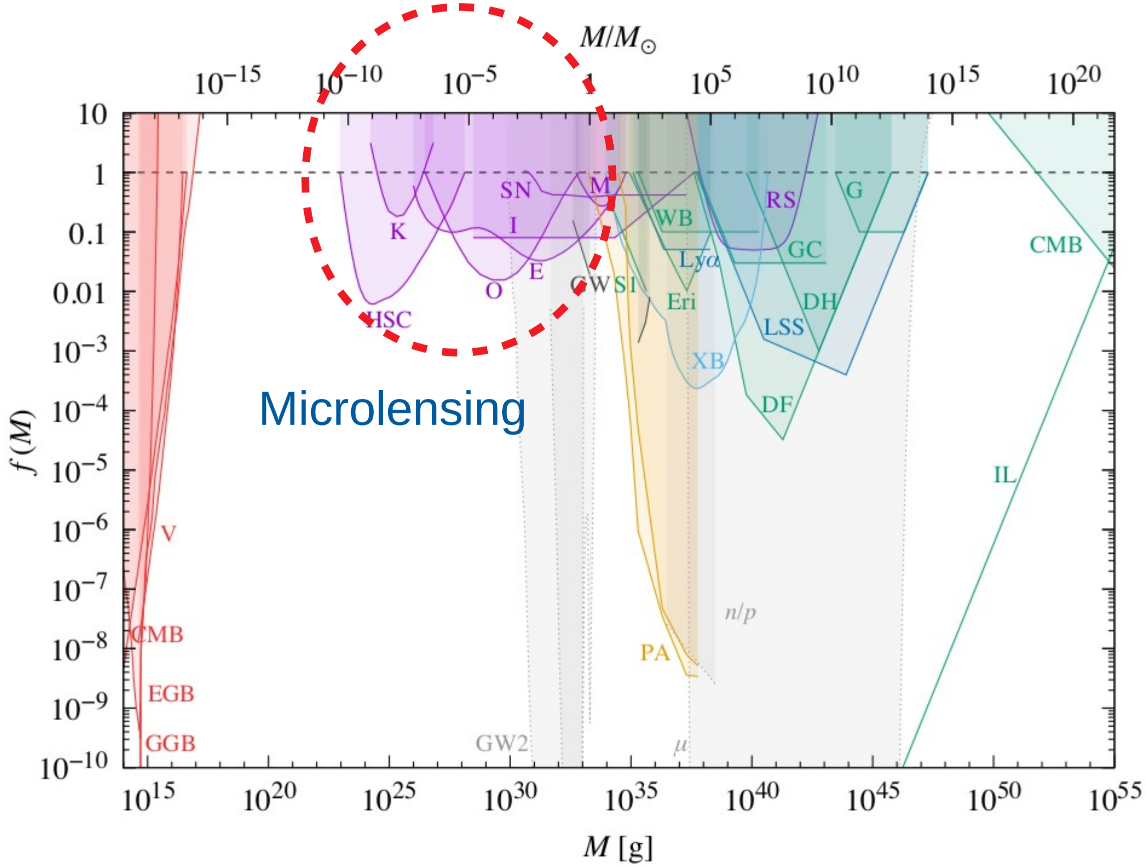

FIG. 10. Constraints on $f(M)$ from evaporation (red), lensing (magenta), dynamical effects (green), gravitational waves (black), accretion (light blue), CMB distortions (orange), large-scale structure (dark blue) and background effects (grey). Evaporation

PBH constraints

- Bounds on the PBH fraction:

B.Carr, K.Kohri,Y.Sendouda,J.Yokoyama: 2002.12778

Hawking evaporation

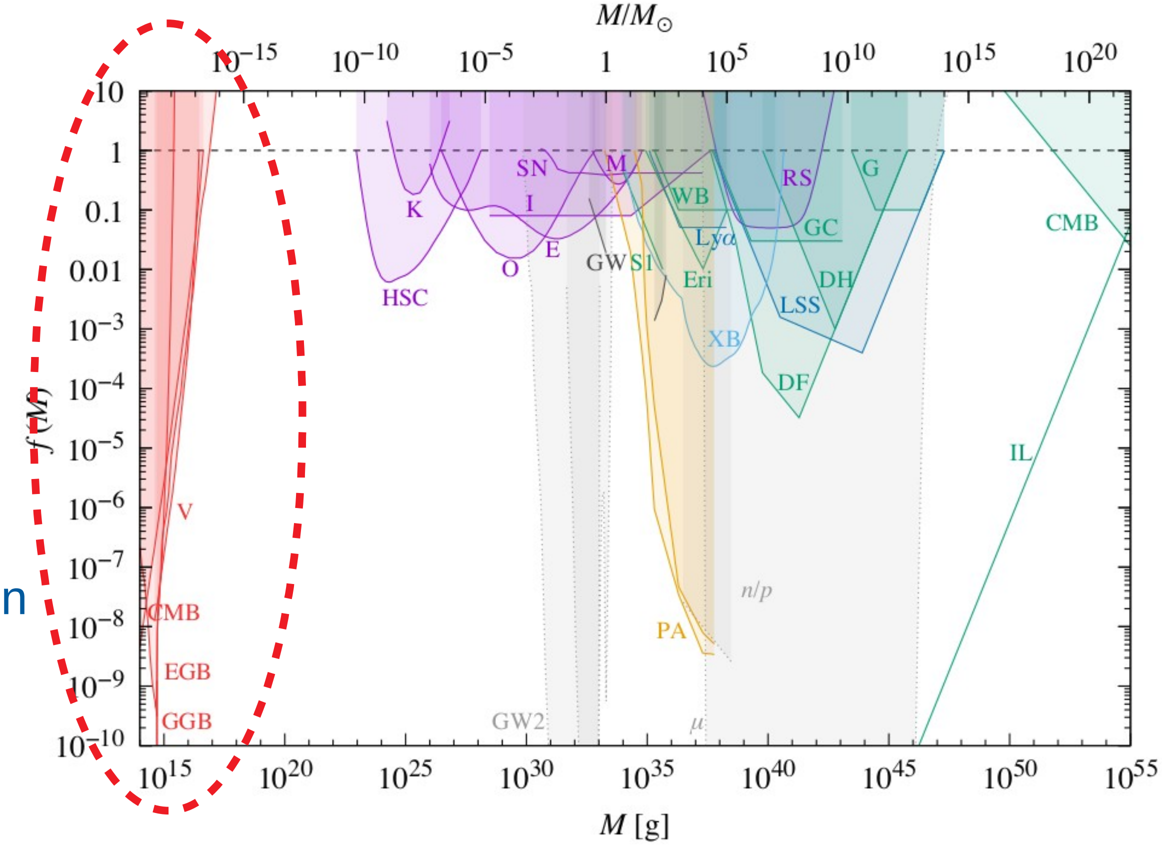

FIG. 10. Constraints on $f(M)$ from evaporation (red), lensing (magenta), dynamical effects (green), gravitational waves (black), accretion (light blue), CMB distortions (orange), large-scale structure (dark blue) and background effects (grey). Evaporation

PBH constraints: Hawking evaporation

- Hawking temperature characterizes black-body spectrum from PBH evaporation

$$T_{\rm PBH} \simeq 5.3\ {\rm MeV} \times \left(\frac{10^{-18} M_\odot}{M_{\rm PBH}}\right)$$

$$\beta(M) \equiv \frac{\rho_{\rm PBH}(t_i)}{\rho(t_i)}$$

$$\beta'(M) \equiv \gamma^{1/2} \left(\frac{g_{*i}}{106.75}\right)^{-1/4} \left(\frac{h}{0.67}\right)^{-2} \beta(M)$$

$$M \approx 1.35 \times 10^9 \left(\frac{f(M)}{15.35}\right)^{1/3} \left(\frac{\tau}{1\,{\rm s}}\right)^{1/3} {\rm g}$$

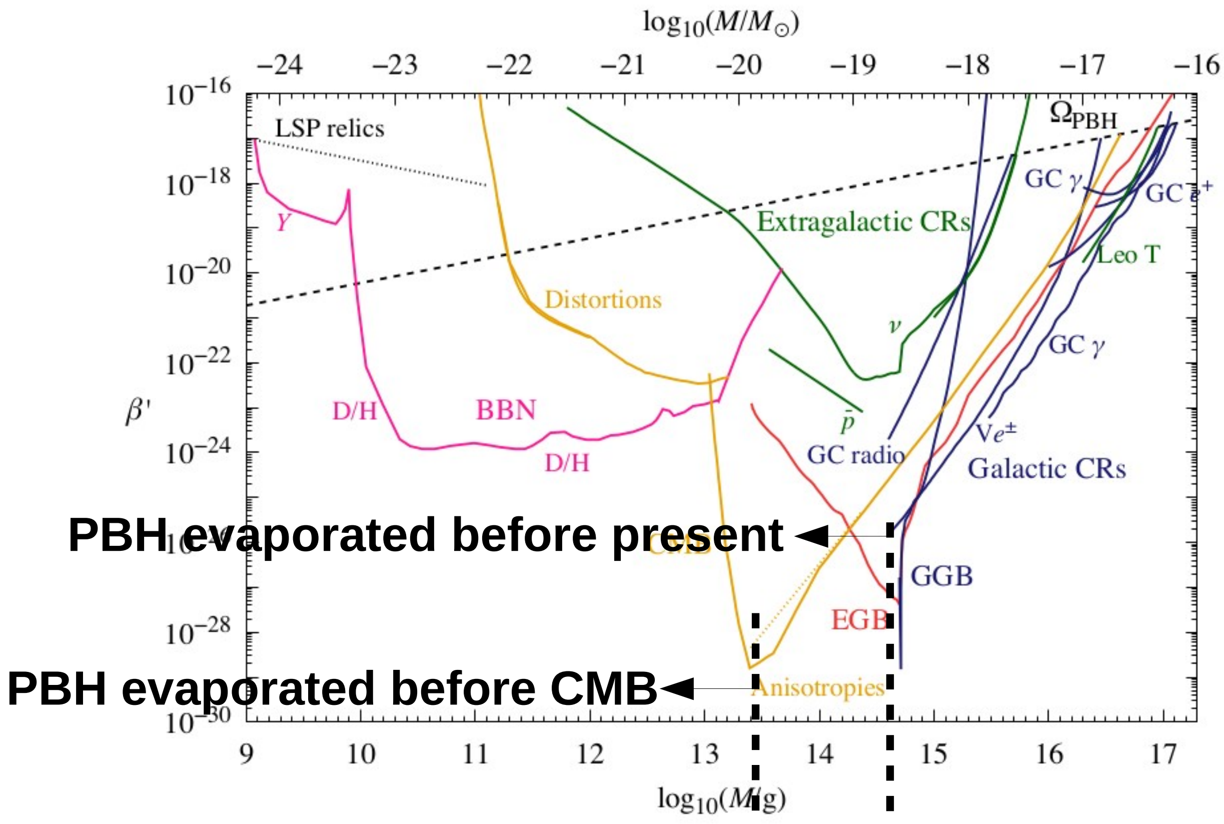

BlackHawk v2.1, A.Aarbey, J.Auffinger: 2108.02737

B.Carr, K.Kohri,Y.Sendouda,J.Yokoyama: 2002.12778

Contents

- Introduction
- 511keV line
- Type Ia Supernovae
- PBH formation
- Boosted DM
- Summary

511 keV line from Galaxy Center

511 keV line excess

- All-Sky map of 511 keV gamma-ray line from INTEGRAL

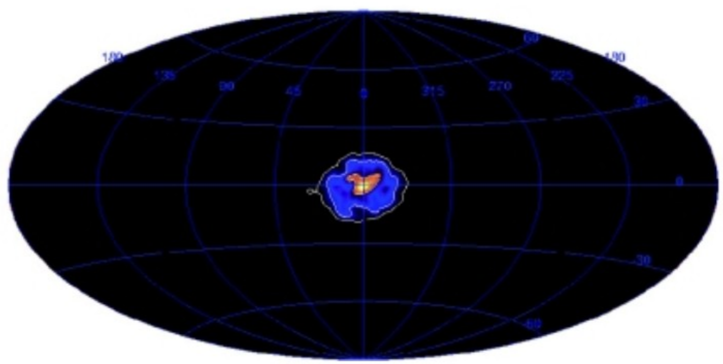

Date: 16 October 2007

Satellite: INTEGRAL

Depicts: Sky map of 511 keV electron-positron annihiliation emission line

Copyright: J. Knödlseder et al.

https://sci.esa.int/web/integral/-/41415-all-sky-map-of-511-kev-line-emission

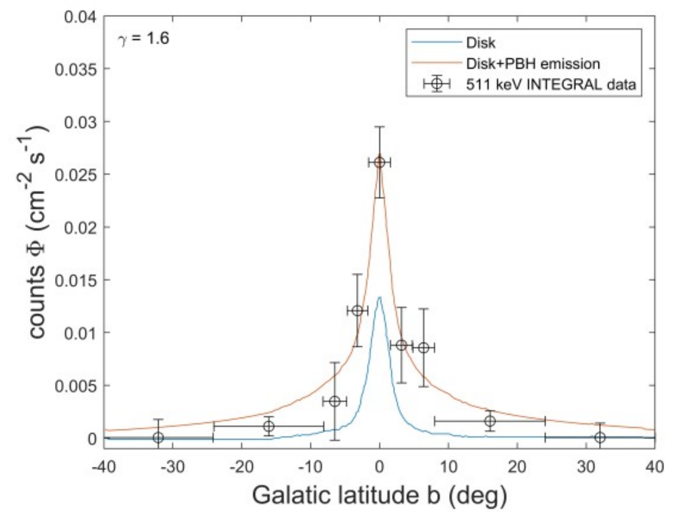

Figure 1. The orange curve is combined 511 keV gamma-ray flux from PBH evaporation with $M_{\rm PBH} = 10^{16}$ g, $f_{\rm PBH} = 10^{-4}$ and astrophysical source [52] (blue curve). Comparing to the INTEGRAL data from 508.25 keV to 513.75 keV [27].

P.Y.Tseng,Y.M.Yeh: 2209.01552

$$\boxed{e^+ + e^- \to \gamma\gamma}$$

- If identified as electron-positron annihilation, it requires the injection rate of 2E43 non-relativistic positrons per second.

PBH interpretation: 511 keV

- We consider PBH mass range from 1E15 to 2E17 g and spectra of evaporated particles (photon, electron, and positron). P.Y.Tseng,Y.M.Yeh: 2209.01552
- 95% positrons from PBH evaporation become non-relativistic via ionization. Among them, 97% form a positronium (e+ e- bound state). 25% of positronium annihilate to a pair of 511 keV photons.

$$\boxed{\Phi_{\rm PBH}(\Delta\Omega) = \frac{0.55 L_{e^+}(M_{\rm PBH}) f_{\rm PBH}}{4\pi M_{\rm PBH}} \int_{\Delta\Omega}\int_{\rm l.o.s} \rho(\ell,\Omega)\, d\ell\, d\Omega}$$

- PBH spatial distribution follow NFW profile:

$$\boxed{\rho(r) = \frac{\rho_0}{(r/R_s)^\gamma[1+(r/R_s)^\alpha]^{(\beta-\gamma)/\alpha}}}$$

PBH interpretation: 511 keV

- We consider PBH mass range from 1E15 to 2E17 g and spectra of evaporated particles (photon, electron, and positron). P.Y.Tseng,Y.M.Yeh: 2209.01552

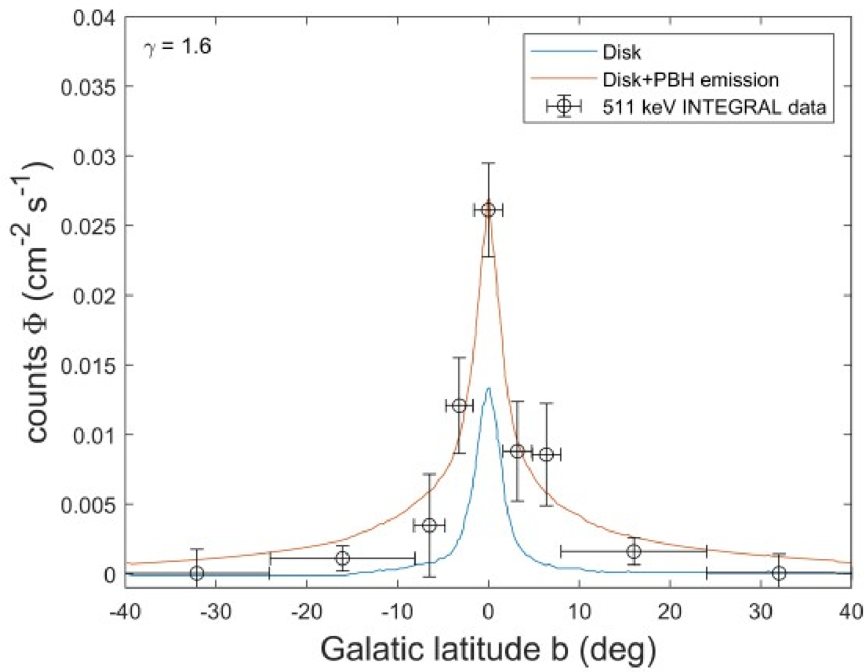

Figure 1. The orange curve is combined 511 keV gamma-ray flux from PBH evaporation with $M_{\rm PBH} = 10^{16}$ g, $f_{\rm PBH} = 10^{-4}$ and astrophysical source [52] (blue curve). Comparing to the INTEGRAL data from 508.25 keV to 513.75 keV [27].

Extra-galactic and Galactic gamma-ray

- There are constraints from extragalactic and galactic continuous gamma-ray spectra. P.Y.Tseng,Y.M.Yeh: 2209.01552

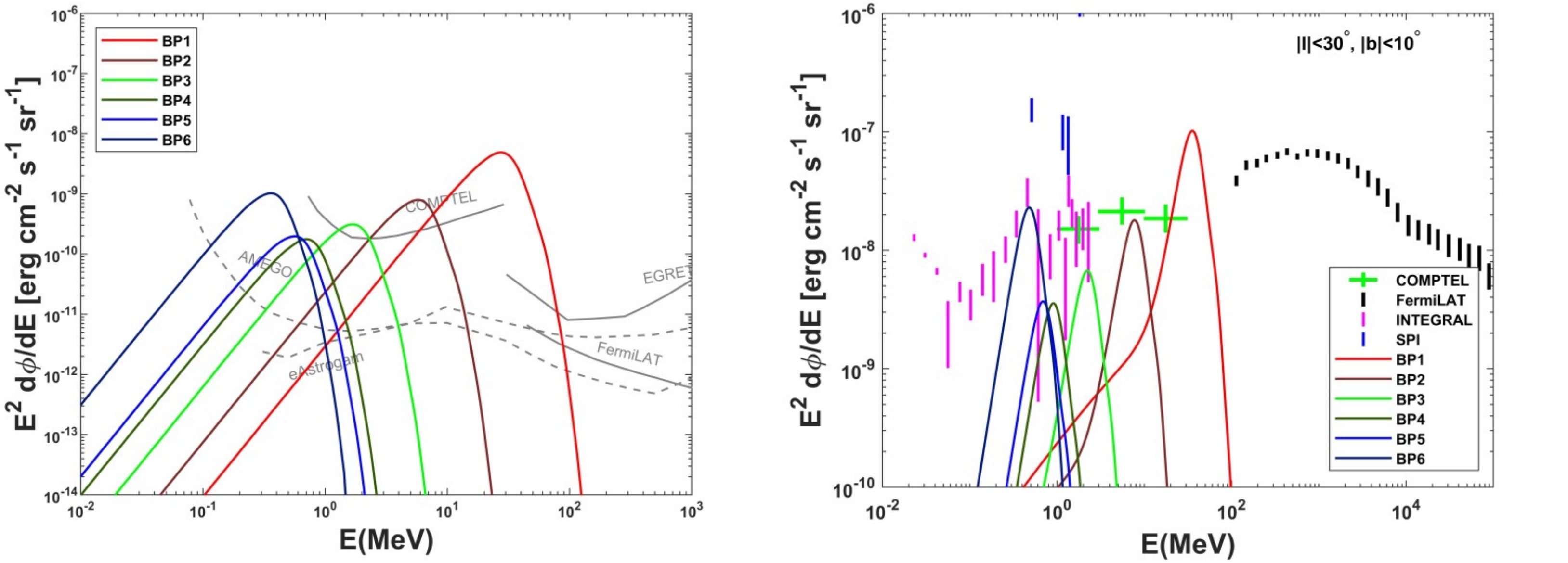

Figure 3. The predicted photon fluxes from the **BP**s listed in table 1 for extragalactic (left-panel) and inner Galactic (right-panel). The current limits from COMPTEL/EGRET/FermiLAT [28] and projecting sensitivities of AMEGO/e-ASTROGAM [29–31] are shown in gray curves in left-panel, meanwhile, in the right-panel, the **BP**s fluxes are compared with the INTEGRAL/SPI/COMPTEL/FermiLAT inner Galactic data ($|l| < 30°$, $|b| < 10°$) [29].

Allowed PBH mass and abundance

- Favored regions of PBHs, interpreting 511 keV excess:

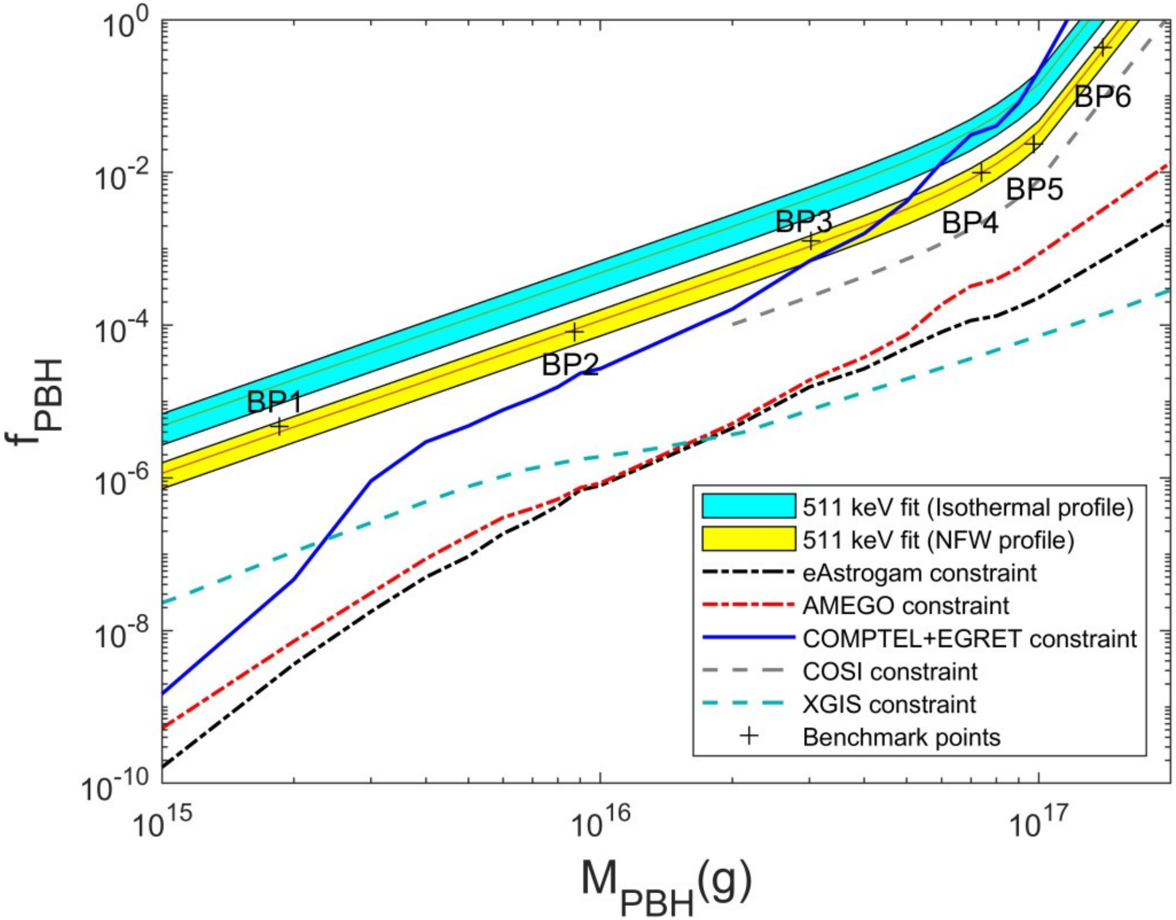

P.Y.Tseng,Y.M.Yeh: 2209.01552

Allowed PBH mass and abundance

- Favored regions of PBHs, interpreting 511 keV excess:

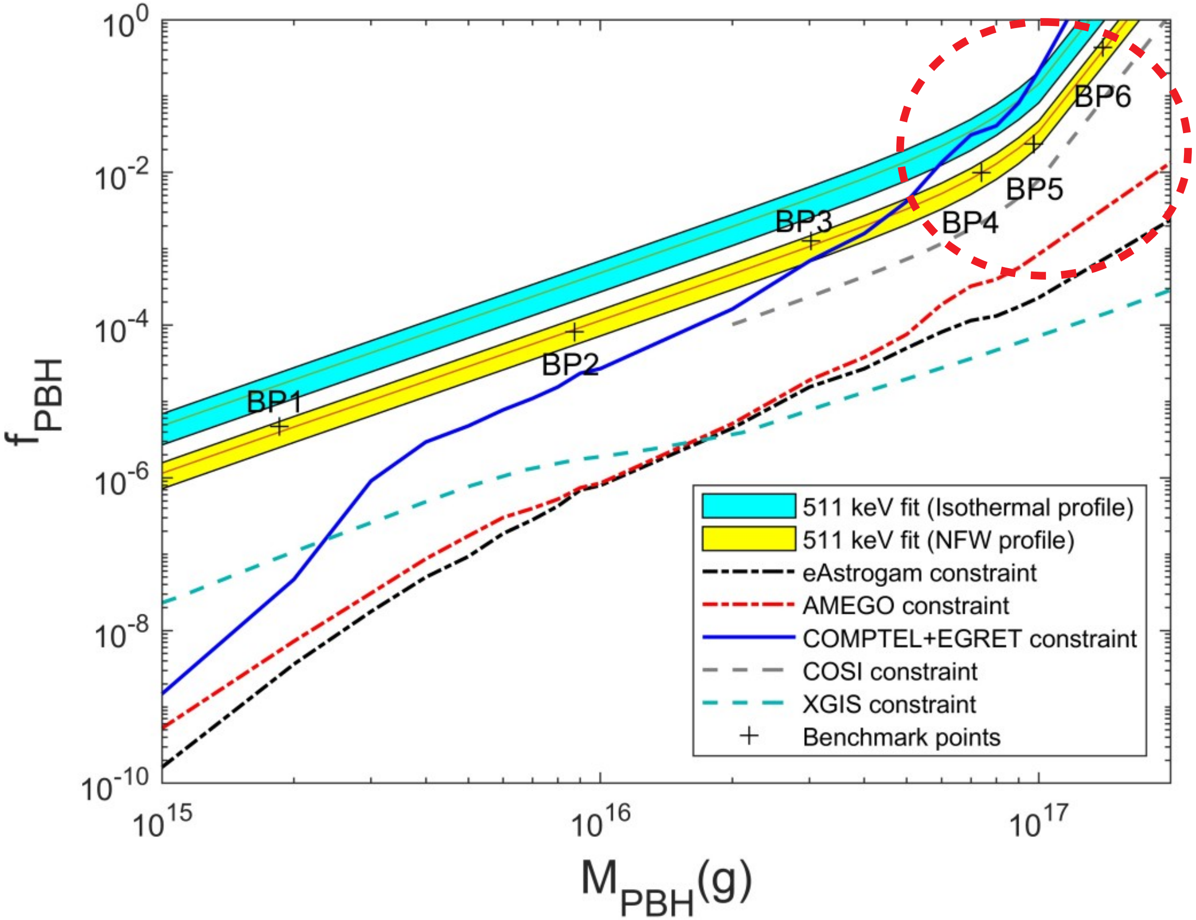

P.Y.Tseng,Y.M.Yeh: 2209.01552

PBH trigger Type Ia Supernovae

PBH constraints

- Mass range of PBH (Primordial Black Holes):

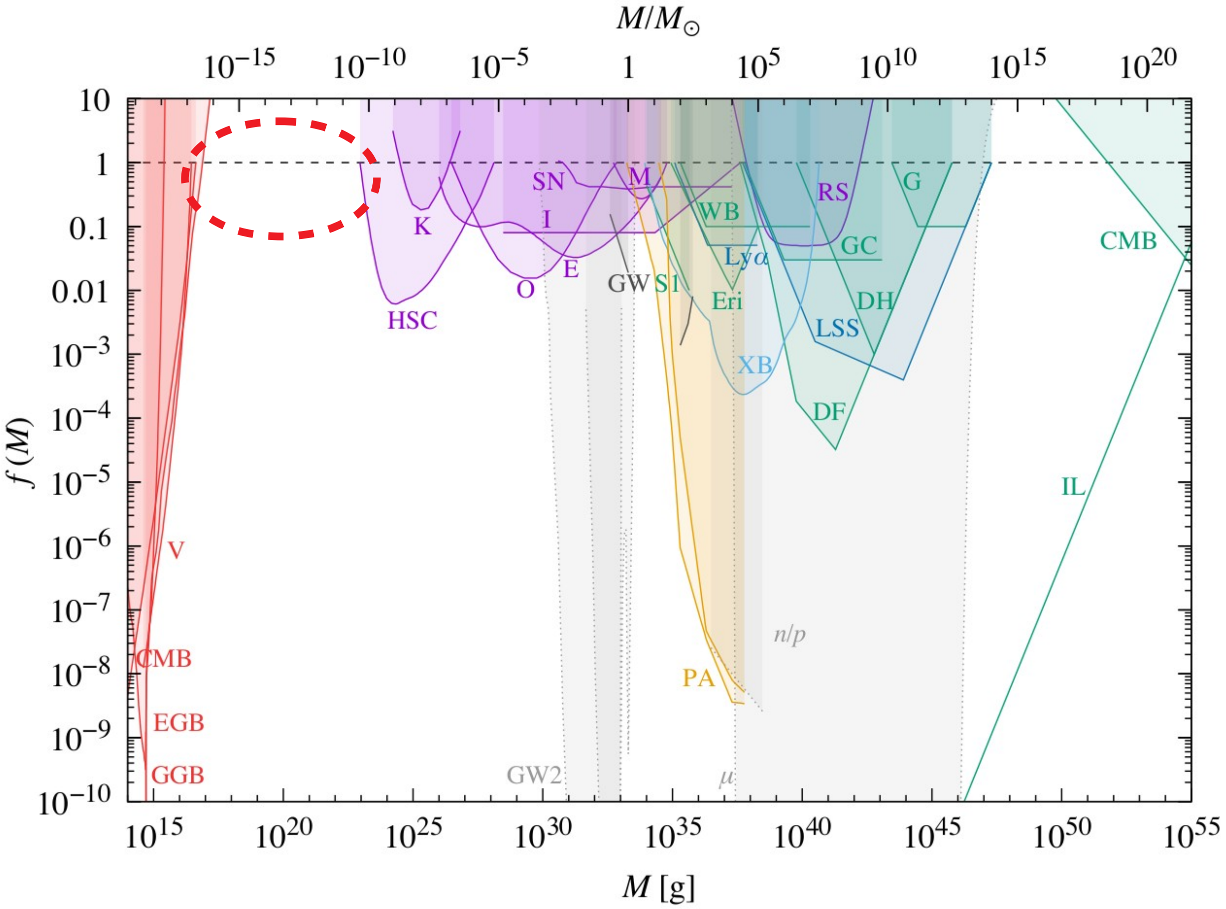

B.Carr, K.Kohri, Y.Sendouda, and J.Yokoyama, arXiv:2002.12778

PBH: Type Ia Supernovae

- An asteroid-mass PBH passes through a white dwarf(WD), which creates a shock wave (Bondi-Hoyle-Lyttleton BHL accretion), such that initiates the thermonuclear supernovae (SN Ia). H.Steigerwalc, E.Tejeda, arXiv:2104.07066
- The maximum radius inside WD associates with detonation ignition R_m , were determined from successful shock wave and self-sustained ignition detonation in the BHL accretion flow.

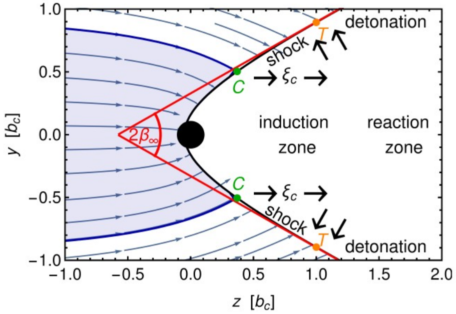

$$\pi R_m^2 \left(\frac{v_{*\mathrm{esc}}(R_m)}{v_{\mathrm{gal}}} \right)^2$$

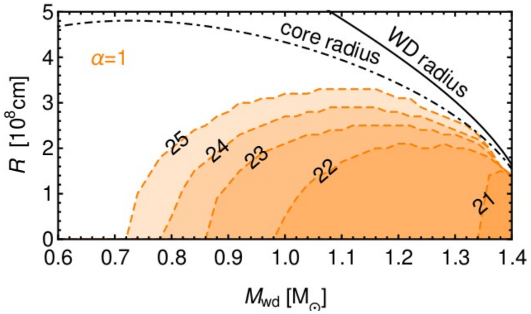

PBH: Type Ia Supernovae

- SN Ia data is able to constrain the fraction of asteroid PBH abundance. P.J.Chen, P.Y.Tseng, arXiv:2305.14399
- We assume the WD distribution follows the stellar distribution, and normalize it to the WD data within 100 pc near our solar system.

$$\frac{dn_{\rm WD}}{dM_{\rm WD}}(R_{\rm MW}, Z_{\rm MW}) = \left.\frac{dn_{\rm WD}}{dM_{\rm WD}}\right|_{\odot} \times \left(e^{R_1/L_1} \exp\left(-\frac{R_{\rm MW}}{L_1} - \frac{|Z_{\rm MW}|}{H_1}\right)\right)$$

$$\left.\frac{dn_{\rm WD}}{dM_{\rm WD}}\right|_{\odot} \equiv \frac{1}{(0.1\,{\rm kpc})^3} \left.\frac{dN_{\rm DM}}{dM_{\rm DM}}\right|_{\rm Fig13}$$

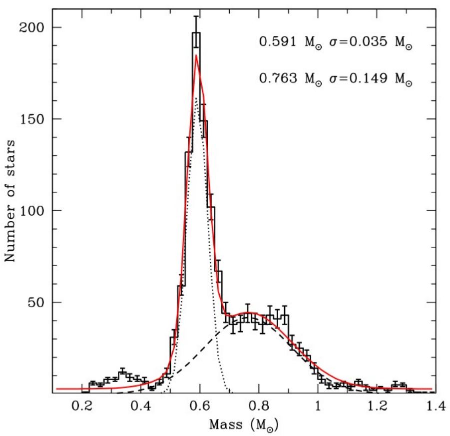

Mukremin Kilic et.al, arXiv:2006.00323

PBH: Type Ia Supernovae

- The observed SN Ia Milky Way event rate is 0.54+-0.12 per century with 68.3% confidence.
- This prefers the certain abundance for asteroid PBH:

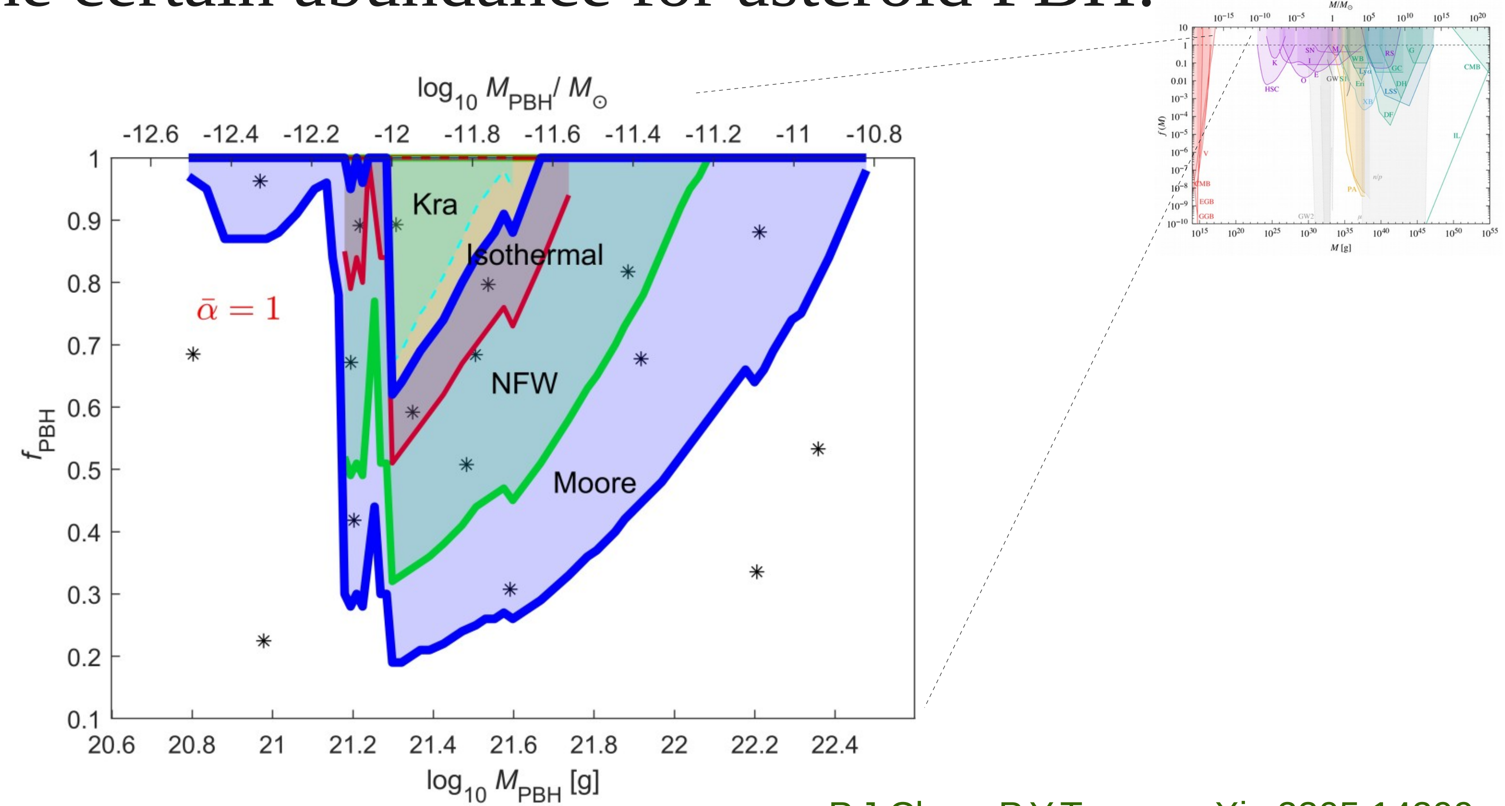

P.J.Chen, P.Y.Tseng, arXiv:2305.14399

PBH formation:

FOPT→FB→PBH

Model framework

- The mass of dark fermion χ come from the vacuum expectation value (vev) inducing by scalar ϕ .

$$\mathcal{L} \supset \bar{\chi}(i\partial\!\!\!/ - m)\chi - g_\chi \phi \bar{\chi}\chi - V_{\rm eff}(\phi, T)$$

$$m_\chi = m + g_\chi v_\phi, \quad v_\phi \equiv \langle \phi \rangle$$

- The finite-temperature **quartic effective potential** induce the first-order phase transition (FOPT) in the early Universe.

$$V_{\rm eff}(\phi, T) = D(T^2 - T_0^2)\phi^2 - (AT + C)\phi^3 + \frac{\lambda}{4}\phi^4$$

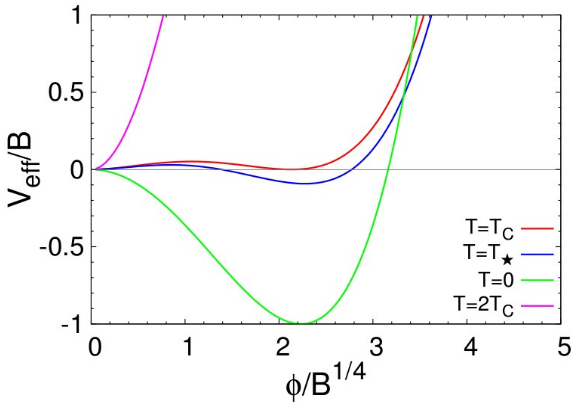

K.Kawana, K.P.Xie: 2106.00111, D.Marfatia, P.Y. Tseng: 2107.00859

First-order phase transition

- More rich phenomenologies, if we consider **1st order phase transition (FOPT)**.

K.Kawana, K.P.Xie: 2106.00111

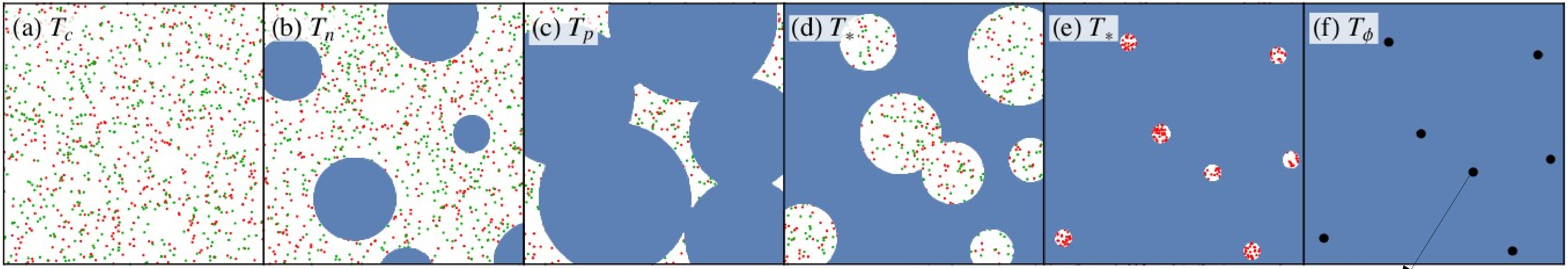

- Dark fermion χ **inside** the bubble becomes the DM relic density (bubble filtering χ).

- χ **outside** the bubble could form macroscopic DM (Fermi Ball or primordial black hole)

Number density of FB

- FBs start to form at $T_\star$ in the false vacuum, it shrinks and separates into smaller volumes.

- Critical volume $V_\star = 4\pi R_\star^3/3$, there is no other bubble forming inside during its shrinking $\Gamma(T_\star)V_\star\Delta t \sim 1$, corresponds to one FB.

- The number density of FB $n_{\rm FB}|_{T_\star}$ is determined by
  $n_{\rm FB}|_{T_\star} V_\star = F(t_\star)$:
  $$\boxed{n_{\rm FB}|_{T_\star} = \left(\frac{3}{4\pi}\right)^{1/4}\left(\frac{\Gamma(T_\star)}{v_w}\right)^{3/4} F(t_\star)}$$

- Total numbers of χ for a FB: $\boxed{Q_{\rm FB} = \eta_\chi \left(\frac{s}{n_{\rm FB}}\right)_{T_\star}}$

FB mass profile

- The mass and radius of FB are obtained by minimizing the FB energy with respect to the radius $dE_{\rm FB}/dR = 0$:

$$E_{\rm FB} = \frac{3\pi}{4}\left(\frac{3}{2\pi}\right)^{2/3}\frac{Q_{\rm FB}^{4/3}}{R}\left[1+\frac{4\pi}{9}\left(\frac{2\pi}{3}\right)^{1/3}\frac{R^2T^2}{Q_{\rm FB}^{2/3}}\right] - \frac{3g_\chi^2}{8\pi}\frac{Q_{\rm FB}^2L_\phi^2}{R^3} + \frac{4\pi}{3}V_0(T)R^3$$

$$R_{\rm FB} = \left[\frac{3}{16}\left(\frac{3}{2\pi}\right)^{2/3}\frac{Q_{\rm FB}^{4/3}}{V_0}\right]^{1/4}\left[1-\frac{\pi}{6\sqrt{3}}\frac{T^2}{V_0^{1/2}}\right]^{1/2},$$

$$M_{\rm FB} = Q_{\rm FB}\,(12\pi^2V_0)^{1/4}\left(1+\frac{\pi}{4\sqrt{3}}\frac{T^2}{V_0^{1/2}}\right),$$

- FB relic abundance: $\Omega_{\rm FB}h^2 = \dfrac{M_{\rm FB}\,n_{\rm FB}|_{T_0}}{3M_{\rm Pl}^2(H_0/h)^2}$

FB collapse to PBH

- The mass and radius of FB are obtained by minimizing the FB energy with respect to the radius $dE_{\rm FB}/dR = 0$:

$$\boxed{E_{\rm FB} = \frac{3\pi}{4}\left(\frac{3}{2\pi}\right)^{2/3}\frac{Q_{\rm FB}^{4/3}}{R}\left[1+\frac{4\pi}{9}\left(\frac{2\pi}{3}\right)^{1/3}\frac{R^2T^2}{Q_{\rm FB}^{2/3}}\right] - \frac{3g_\chi^2}{8\pi}\frac{Q_{\rm FB}^2 L_\phi^2}{R^3} + \frac{4\pi}{3}V_0(T)R^3}$$

$$\boxed{L_\phi(T) \equiv \left(\left.\frac{d^2V_{\rm eff}}{d\phi^2}\right|_{\phi=0}\right)^{-1/2} = \left(2D(T^2-T_0^2)\right)^{-1/2}}$$

- Magnitude of Yukawa energy increases as FB temperature decrease. It will dominate when $L_\phi \simeq R_{\rm FB}/Q_{\rm FB}^{1/3}$, and FB collapse to PBH.

Boosted Dark matter from PBH evaporation

Boosted DMs from PBH evaporation

- Hawking temperature characterizes black-body spectrum from PBH evaporation:

BlackHawk v2.1, A.Aarbey, J.Auffinger: 2108.02737

$$\boxed{T_{\rm PBH} \simeq 5.3~{\rm MeV} \times \left(\frac{10^{-18} M_\odot}{M_{\rm PBH}}\right)}$$

$$\boxed{\frac{dN_\chi}{d\mathcal{T}dt} = \frac{2\Gamma_\chi(\mathcal{T}, M_{\rm PBH})}{\pi(e^{(\mathcal{T}+m_\chi)/T_{\rm PBH}}+1)}}$$

- χ flux on Earth come from extragalactic PBH, it does not rely on DM density near galactic center

$$\frac{d\Phi}{d\mathcal{T}} = \int_{t_\phi}^{\min(t_{\rm eva}, t_0)} c\, dt[1+z(t)]\frac{f_{\rm PBH}\rho_{\rm DM}}{M_{\rm PBH}}\frac{d^2N_\chi}{d\mathcal{T}dt}\bigg|_{\tilde{E}=\sqrt{(E^2-m_\chi^2)(1+z(t))^2+m_\chi^2}}$$

R.Calabrese et. al: 2203.17093

DM-e scattering

- We are interested in χ in energy range from keV to GeV so that XENON1T/XENONnT and SK/HK can detect a signal.

$$\frac{d\sigma}{dE_r} = \frac{\sigma_{\chi e}\Theta(E_r^{\max} - E_r)}{8\mu_{\chi e}^2 \tilde{p}^2}(2m_e + E_r)(2m_\chi^2 + m_e E_r)$$

- The maximum allowed recoil energy

$$E_r^{\max} = \frac{2m_e \mathcal{T}(\mathcal{T} + 2m_e)}{((m_e + m_\chi)^2 + 2m_e \mathcal{T})}$$

At XENON1T/XENONnT

- At XENON1T/XENONnT detector, χ can ionize the Xe atom via $\chi + \mathrm{Xe} \rightarrow \chi + \mathrm{Xe}^{*} + e^{-}$, which produces an electron recoil signal.

XENON Collaboration: 2207.11330, 2006.09721

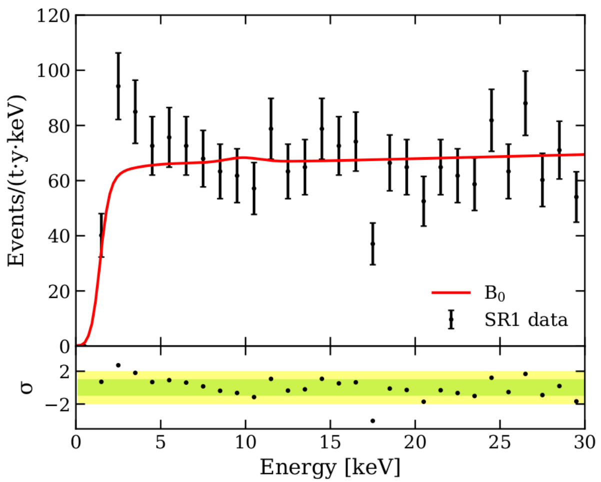

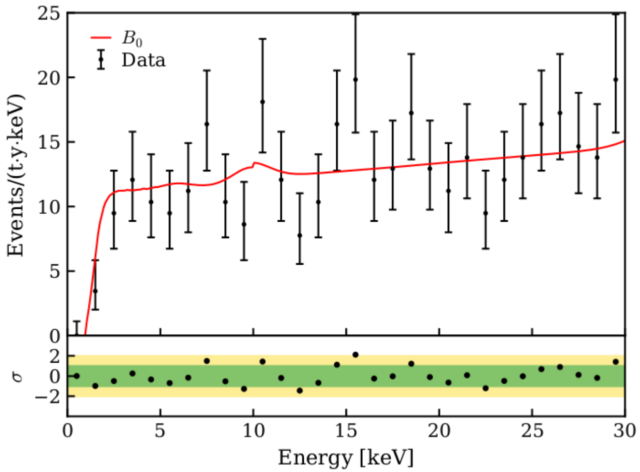

- XENONnT reduced tritium background five times lower than in XENON1T.

At XENON1T/XENONnT

- At XENON1T/XENONnT detector, the differential event rate is given by

$$\boxed{\frac{dR}{dE_r} = n_t\, \eta(E_r)\, \tilde{F}(E_r) \int d\mathcal{T} \frac{d\Phi}{d\mathcal{T}} \sum_{n,l} \frac{d\sigma^{n,l}}{dE_r}}$$

including the cross section of scattering of χ on a bound electron, because the binding energy is non-negligible compared to energy of χ .

R.Calabrese et. al: 2203.17093

- To find parameter space allowed by data

$$\chi^2 \equiv \sum_i \left(\frac{\left.\frac{dR}{dE_r}\right|_i + \left.\frac{dR_{\rm bkgd}}{dE_r}\right|_i - \left.\frac{dR_{\rm obs}}{dE_r}\right|_i}{\sigma_i} \right)^2$$

At SK/HK

- At SK/HK, χ-e scattering produce Cherenkov radiation.
- 161.9 kiloton-year SK observed 4042 events, which is compatible with background 3992.9.

Super-Kamiokande: 1711.05278

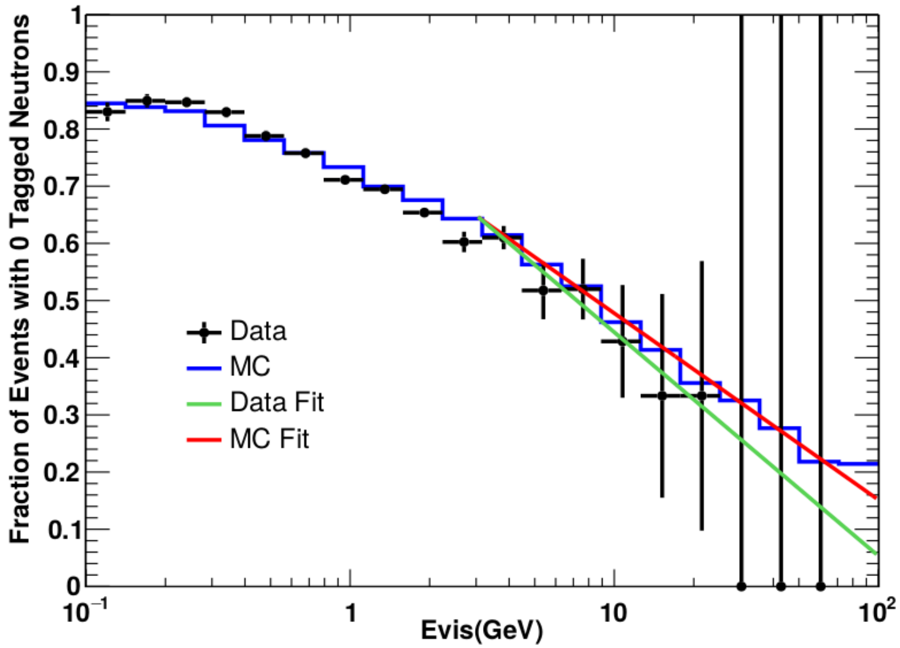

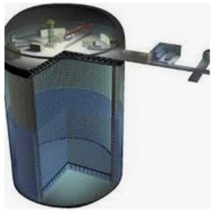

At SK/HK

- At SK/HK, χ-e scattering produce Cherenkov radiation.
- 161.9 kiloton-year SK observed 4042 events , which is compatible with background 3992.9. Super-Kamiokande: 1711.05278

$$\boxed{N_{\rm PBH}^{\rm SK} = 161.9\ [\text{kton} - \text{yr}] \times \int_{0.1\ \text{GeV}}^{1.33\ \text{GeV}} dE_r \frac{dR}{dE_r}}$$

- Define 2σ exclusion by $N_{\rm PBH}^{\rm SK} / \sqrt{N_{\rm PBH}^{\rm SK} + N_{\rm bkgd}^{\rm SK}} \geq 2$.
- HK is expected to collect 3.74 Mton-year exposure.

Hyper-Kamiokande: 1805.04163

Correlated signals

Parameter scan

- This model: dark sector <--> PBH observable
- Specify the quartic effective potential:

$$\boxed{V_{\rm eff}(\phi,T) = D(T^2 - T_0^2)\phi^2 - (AT + C)\phi^3 + \frac{\lambda}{4}\phi^4}$$

- Finding the parameter regime, which realizes the scenario:

$$\begin{aligned} &0.05 \le \lambda \le 0.2\,, \quad 0.1 \le B^{1/4}/\mathrm{MeV} \le 10^4\,, \quad 0.01 \le C/\mathrm{MeV} \le 10^4\,,\\ &0.1 \le D \le 10\,, \quad 0.3 \le T_\star/T_{\mathrm{SM}\star} \le 1.0\,, \quad 0.01 \le g_\chi \le \sqrt{4\pi}\,,\\ &10^{-3} \le m/B^{1/4} \le 10\,, \quad 10^{-40} \le \sigma_{\chi e}/\mathrm{cm}^2 \le 10^{-31}\,. \end{aligned}$$

Gravitational Wave

D.Marfatia, P.Y.Tseng: 2112.14588

- GW spectra from the benchmark points:

	BP-1	BP-2	BP-3	BP-4	BP-5	BP-6
λ	0.161	0.103	0.185	0.189	0.196	0.171
$B^{1/4}/\mathrm{MeV}$	1.796	4.237	0.294	10.75	0.499	1.171
C/MeV	0.065	0.113	0.021	1.736	0.079	0.115
D	3.676	6.910	4.189	1.017	0.441	1.538
g_χ	1.698	1.011	1.375	1.306	1.808	1.663
η_χ	7.62×10^{-13}	3.35×10^{-13}	3.13×10^{-16}	5.92×10^{-16}	3.23×10^{-18}	3.48×10^{-17}
m/MeV	0.021	0.344	0.028	20.54	0.059	0.016
$\sigma_{\chi e}/\mathrm{cm}^2$	8.80×10^{-32}	5.85×10^{-32}	8.62×10^{-33}	1.40×10^{-32}	1.99×10^{-33}	6.44×10^{-32}
$T_{\mathrm{SM}\star}/\mathrm{MeV}$	0.909	2.252	0.189	14.86	0.737	0.991
$T_\star/\mathrm{MeV}$	0.547	0.833	0.074	4.906	0.411	0.489
T_f/MeV	0.591	1.183	0.103	7.846	0.459	0.643
T_ϕ/MeV	0.546	0.823	0.072	4.285	0.391	0.481
T_0/MeV	0.529	0.810	0.069	2.272	0.184	0.401
α	2.21×10^{-2}	2.63×10^{-2}	4.17×10^{-2}	2.73×10^{-2}	2.29×10^{-2}	5.00×10^{-2}
$\beta/H_\star$	3.05×10^{4}	2.30×10^{4}	1.48×10^{4}	1.52×10^{3}	2.13×10^{3}	4.84×10^{3}
v_w	0.873	0.974	0.971	0.985	0.902	0.962
$dM_{\mathrm{FB}}/dQ_{\mathrm{FB}}/\mathrm{MeV}$	2.410	4.859	0.424	42.52	1.890	2.647
$m_\chi(T_\star)/\mathrm{MeV}$	2.949	5.056	0.528	57.19	2.588	3.775
Q_{FB}	2.98×10^{42}	2.27×10^{41}	1.71×10^{42}	7.67×10^{39}	1.28×10^{41}	3.80×10^{40}
R_{FB} [cm]	2876	534	1.21×10^{4}	21.94	1249	461
$\sigma_{\chi\chi}$ [cm^2]	1.06×10^{-21}	3.28×10^{-22}	2.82×10^{-20}	1.19×10^{-23}	1.39×10^{-21}	1.00×10^{-21}
n_χ [cm^{-3}]	2.99×10^{31}	3.56×10^{32}	2.33×10^{29}	1.73×10^{35}	1.57×10^{31}	9.26×10^{31}
$\ell_\chi = 1/n_\chi \sigma_{\chi\chi}$ [cm]	3.16×10^{-11}	8.58×10^{-12}	1.52×10^{-10}	4.85×10^{-13}	4.58×10^{-11}	1.08×10^{-11}
$M_{\mathrm{PBH}}/M_\odot$	6.47×10^{-18}	1.13×10^{-18}	7.64×10^{-19}	3.91×10^{-19}	2.18×10^{-19}	9.34×10^{-20}
β'	2.90×10^{-23}	1.22×10^{-23}	8.40×10^{-28}	1.00×10^{-25}	1.78×10^{-29}	1.80×10^{-28}
$\Omega_{\mathrm{PBH}} h^2$	5.79×10^{-7}	5.53×10^{-7}	4.80×10^{-11}	7.72×10^{-9}	1.91×10^{-12}	2.98×10^{-11}
$f_{\mathrm{PBH}} \times \sigma_{\chi e}/\mathrm{cm}^2$	4.25×10^{-37}	2.70×10^{-37}	3.45×10^{-42}	9.02×10^{-40}	3.16×10^{-44}	1.60×10^{-41}
ΔN_{eff}	0.479	0.200	0.386	0.199	0.409	0.472
$\chi^2\|_{\mathrm{XENON1T}}$	166.82	166.50	167.11	167.78	167.11	167.11
$\chi^2\|_{\mathrm{XENONnT}}$	20.92	20.31	19.95	19.91	19.95	19.95
$\chi^2\|_{\mathrm{XENONnT}_{20\,\mathrm{ton-yr}}}$	**25.76**	**10.93**	0	**14.58**	0	0
N_{SK}	0	14.30	36.14	27.91	115.8	27.56
N_{HK}	0	330	**835**	**645**	**2674**	**637**

Gravitational Wave

D.Marfatia, P.Y.Tseng: 2112.14588

- GW spectra from the benchmark points:

Temperature of FOPT: $T_{\mathrm{SM}\star}$, $T_\star$ rows; DM mass: $m_\chi(T_\star)$ row; PBH mass: $M_{\mathrm{PBH}}/M_\odot$ row.

	BP-1	BP-2	BP-3	BP-4	BP-5	BP-6
λ	0.161	0.103	0.185	0.189	0.196	0.171
$B^{1/4}$/MeV	1.796	4.237	0.294	10.75	0.499	1.171
C/MeV	0.065	0.113	0.021	1.736	0.079	0.115
D	3.676	6.910	4.189	1.017	0.441	1.538
g_χ	1.698	1.011	1.375	1.306	1.808	1.663
η_χ	7.62×10^{-13}	3.35×10^{-13}	3.13×10^{-16}	5.92×10^{-16}	3.23×10^{-18}	3.48×10^{-17}
m/MeV	0.021	0.344	0.028	20.54	0.059	0.016
$\sigma_{\chi e}/\mathrm{cm}^2$	8.80×10^{-32}	5.85×10^{-32}	8.62×10^{-33}	1.40×10^{-32}	1.99×10^{-33}	6.44×10^{-32}
$T_{\mathrm{SM}\star}$/MeV	0.909	2.252	0.189	14.86	0.737	0.991
$T_\star$/MeV	0.547	0.833	0.074	4.906	0.411	0.489
T_f/MeV	0.591	1.183	0.103	7.846	0.459	0.643
T_ϕ/MeV	0.546	0.823	0.072	4.285	0.391	0.481
T_0/MeV	0.529	0.810	0.069	2.272	0.184	0.401
α	2.21×10^{-2}	2.63×10^{-2}	4.17×10^{-2}	2.73×10^{-2}	2.29×10^{-2}	5.00×10^{-2}
$\beta/H_\star$	3.05×10^{4}	2.30×10^{4}	1.48×10^{4}	1.52×10^{3}	2.13×10^{3}	4.84×10^{3}
v_w	0.873	0.974	0.971	0.985	0.902	0.962
$dM_{\mathrm{FB}}/dQ_{\mathrm{FB}}$/MeV	2.410	4.859	0.424	42.52	1.890	2.647
$m_\chi(T_\star)$/MeV	2.949	5.056	0.528	57.19	2.588	3.775
Q_{FB}	2.98×10^{42}	2.27×10^{41}	1.71×10^{42}	7.67×10^{39}	1.28×10^{41}	3.80×10^{40}
R_{FB} [cm]	2876	534	1.21×10^{4}	21.94	1249	461
$\sigma_{\chi\chi}$ [cm^2]	1.06×10^{-21}	3.28×10^{-22}	2.82×10^{-20}	1.19×10^{-23}	1.39×10^{-21}	1.00×10^{-21}
n_χ [cm^{-3}]	2.99×10^{31}	3.56×10^{32}	2.33×10^{29}	1.73×10^{35}	1.57×10^{31}	9.26×10^{31}
$\ell_\chi = 1/n_\chi \sigma_{\chi\chi}$ [cm]	3.16×10^{-11}	8.58×10^{-12}	1.52×10^{-10}	4.85×10^{-13}	4.58×10^{-11}	1.08×10^{-11}
$M_{\mathrm{PBH}}/M_\odot$	6.47×10^{-18}	1.13×10^{-18}	7.64×10^{-19}	3.91×10^{-19}	2.18×10^{-19}	9.34×10^{-20}
β'	2.90×10^{-23}	1.22×10^{-23}	8.40×10^{-28}	1.00×10^{-25}	1.78×10^{-29}	1.80×10^{-28}
$\Omega_{\mathrm{PBH}} h^2$	5.79×10^{-7}	5.53×10^{-7}	4.80×10^{-11}	7.72×10^{-9}	1.91×10^{-12}	2.98×10^{-11}
$f_{\mathrm{PBH}} \times \sigma_{\chi e}/\mathrm{cm}^2$	4.25×10^{-37}	2.70×10^{-37}	3.45×10^{-42}	9.02×10^{-40}	3.16×10^{-44}	1.60×10^{-41}
ΔN_{eff}	0.479	0.200	0.386	0.199	0.409	0.472
$\chi^2\vert_{\mathrm{XENON1T}}$	166.82	166.50	167.11	167.78	167.11	167.11
$\chi^2\vert_{\mathrm{XENONnT}}$	20.92	20.31	19.95	19.91	19.95	19.95
$\chi^2\vert_{\mathrm{XENONnT}_{20\,\mathrm{ton-yr}}}$	**25.76**	**10.93**	0	**14.58**	0	0
N_{SK}	0	14.30	36.14	27.91	115.8	27.56
N_{HK}	0	330	**835**	**645**	**2674**	**637**

Parameter scan

D.Marfatia, P.Y.Tseng: 2112.14588

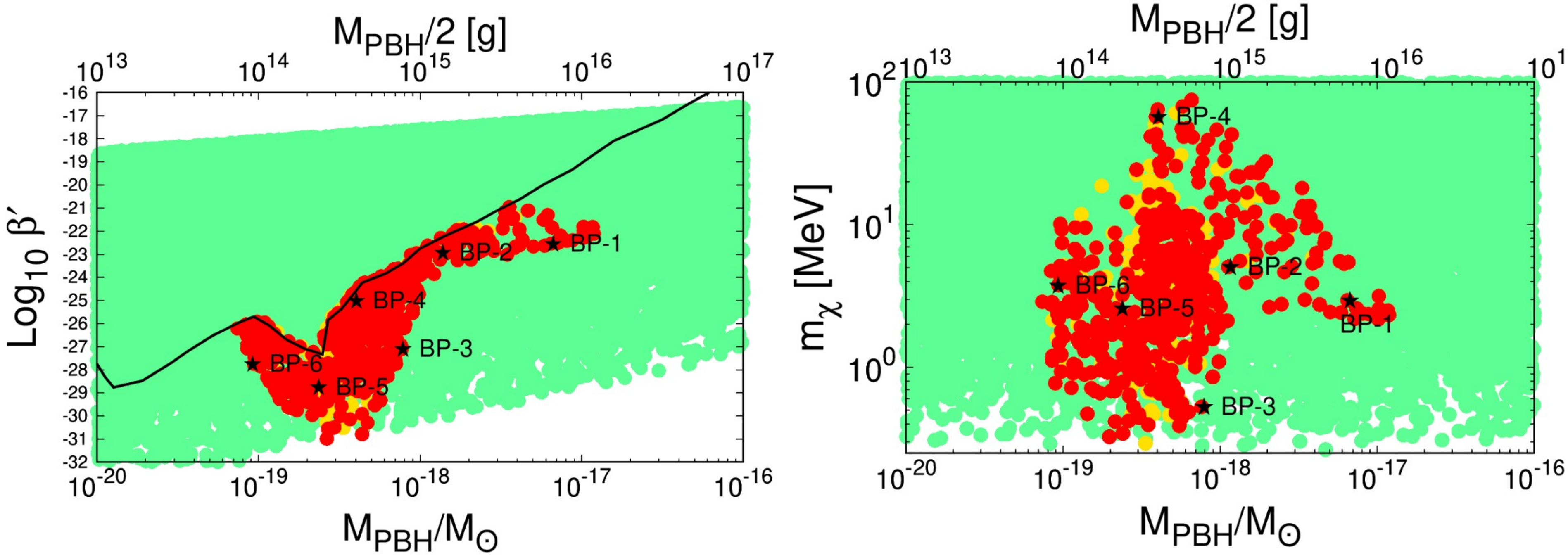

Figure 1. The regions of parameter space that produce a detectable boosted DM flux at XENON1T/XENONnT/SK+GW (yellow), XENONnT/HK+GW (red), and a gravitational wave signal at THEIA/μAres (green).

Parameter scan

D.Marfatia, P.Y.Tseng: 2112.14588

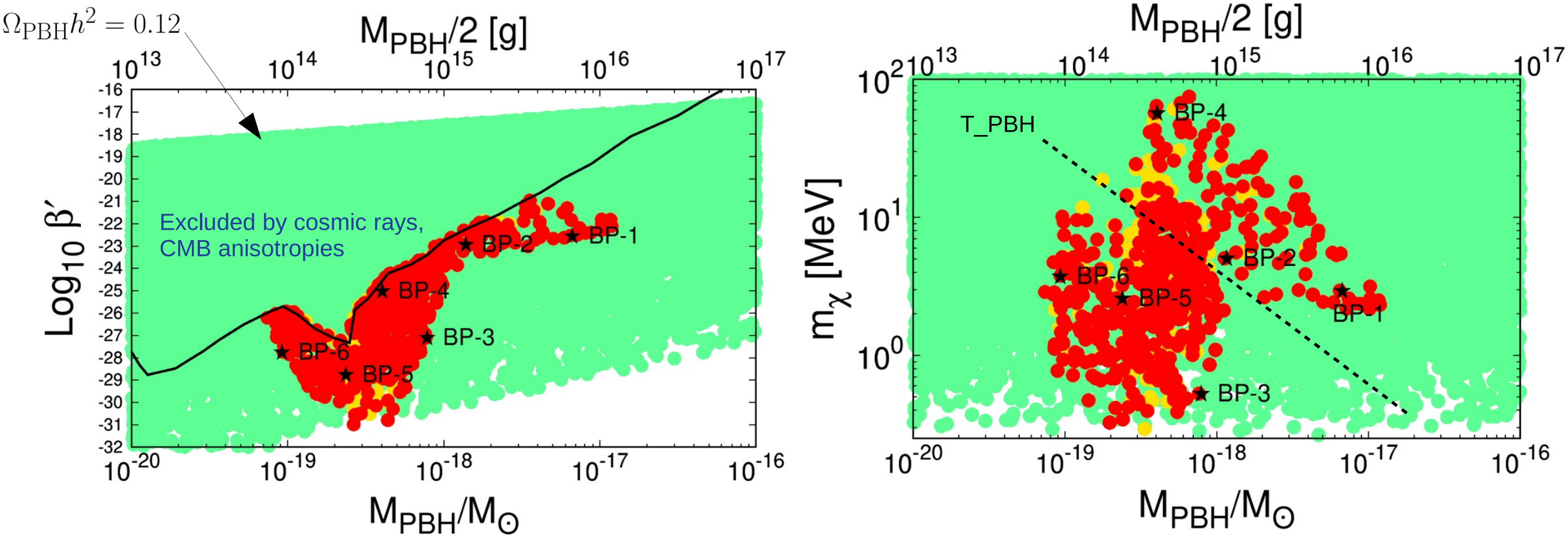

Figure 1. The regions of parameter space that produce a detectable boosted DM flux at XENON1T/XENONnT/SK+GW (yellow), XENONnT/HK+GW (red), and a gravitational wave signal at THEIA/μAres (green).

Parameter scan

D.Marfatia, P.Y.Tseng: 2112.14588

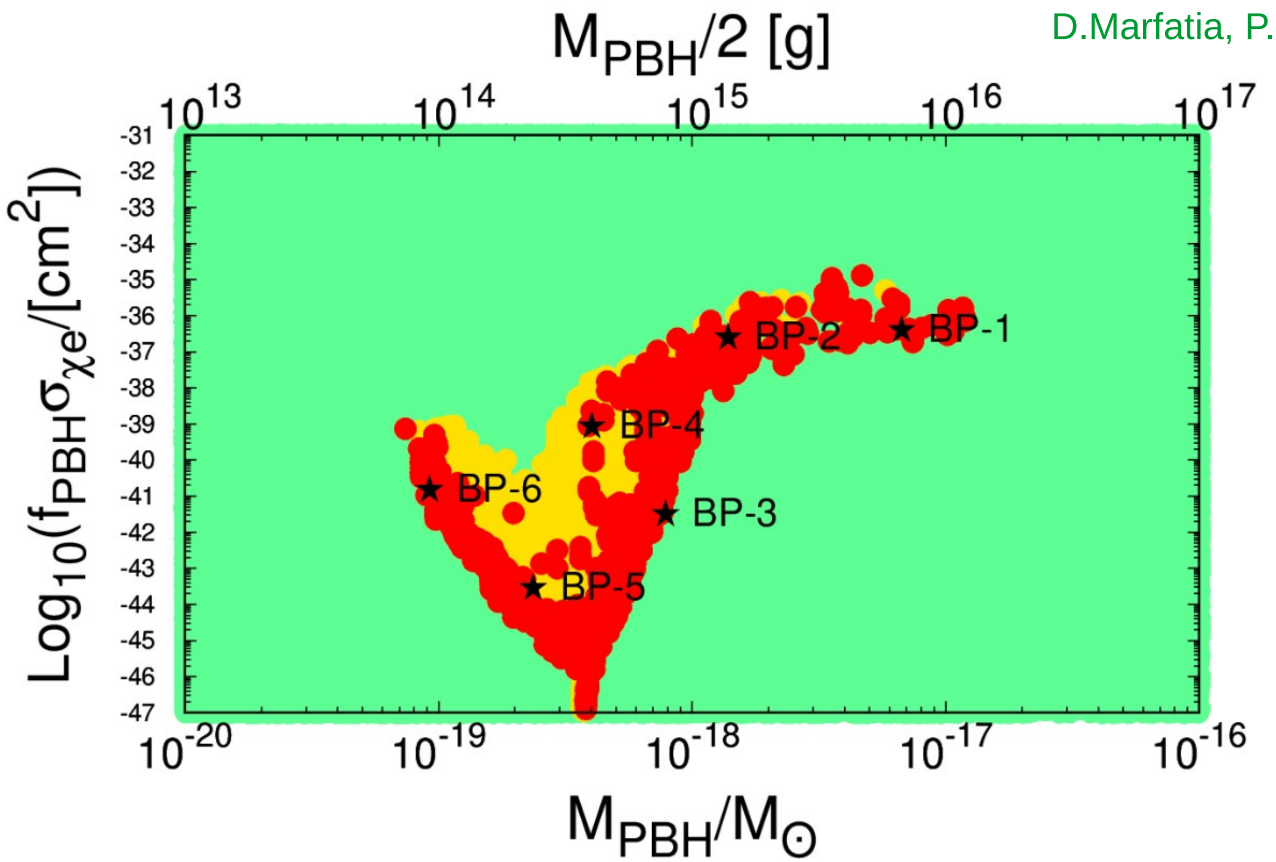

Figure 1. The regions of parameter space that produce a detectable boosted DM flux at XENON1T/XENONnT/SK+GW (yellow), XENONnT/HK+GW (red), and a gravitational wave signal at THEIA/μAres (green).

Parameter scan

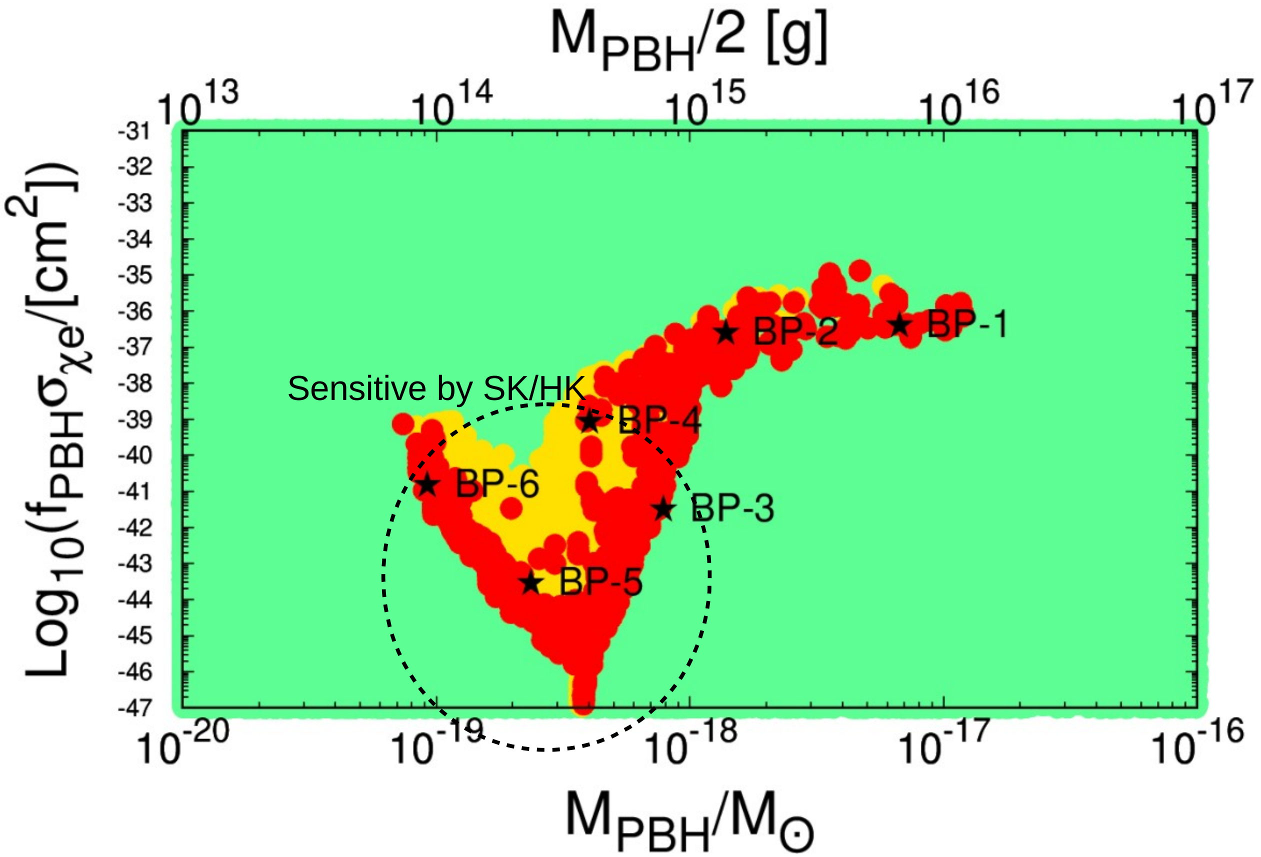

Figure 1. The regions of parameter space that produce a detectable boosted DM flux at XENON1T/XENONnT/SK+GW (yellow), XENONnT/HK+GW (red), and a gravitational wave signal at THEIA/μAres (green).

Parameter scan

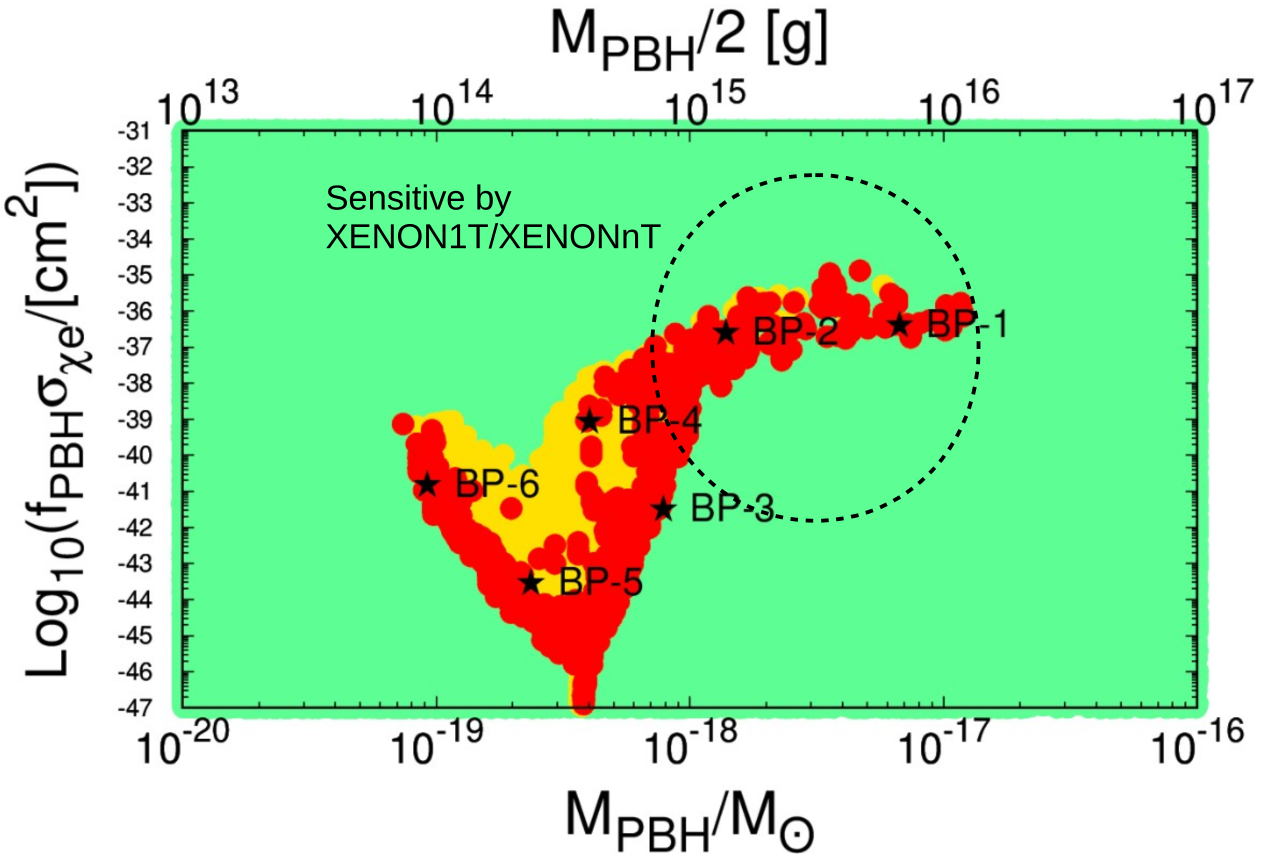

Figure 1. The regions of parameter space that produce a detectable boosted DM flux at XENON1T/XENONnT/SK+GW (yellow), XENONnT/HK+GW (red), and a gravitational wave signal at THEIA/μAres (green).

Gravitational Wave

D.Marfatia, P.Y.Tseng: 2112.14588

- GW spectra from the benchmark points:

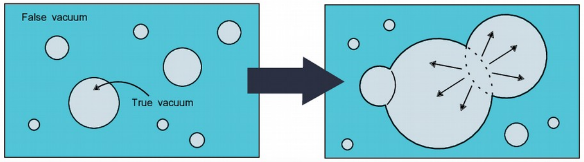

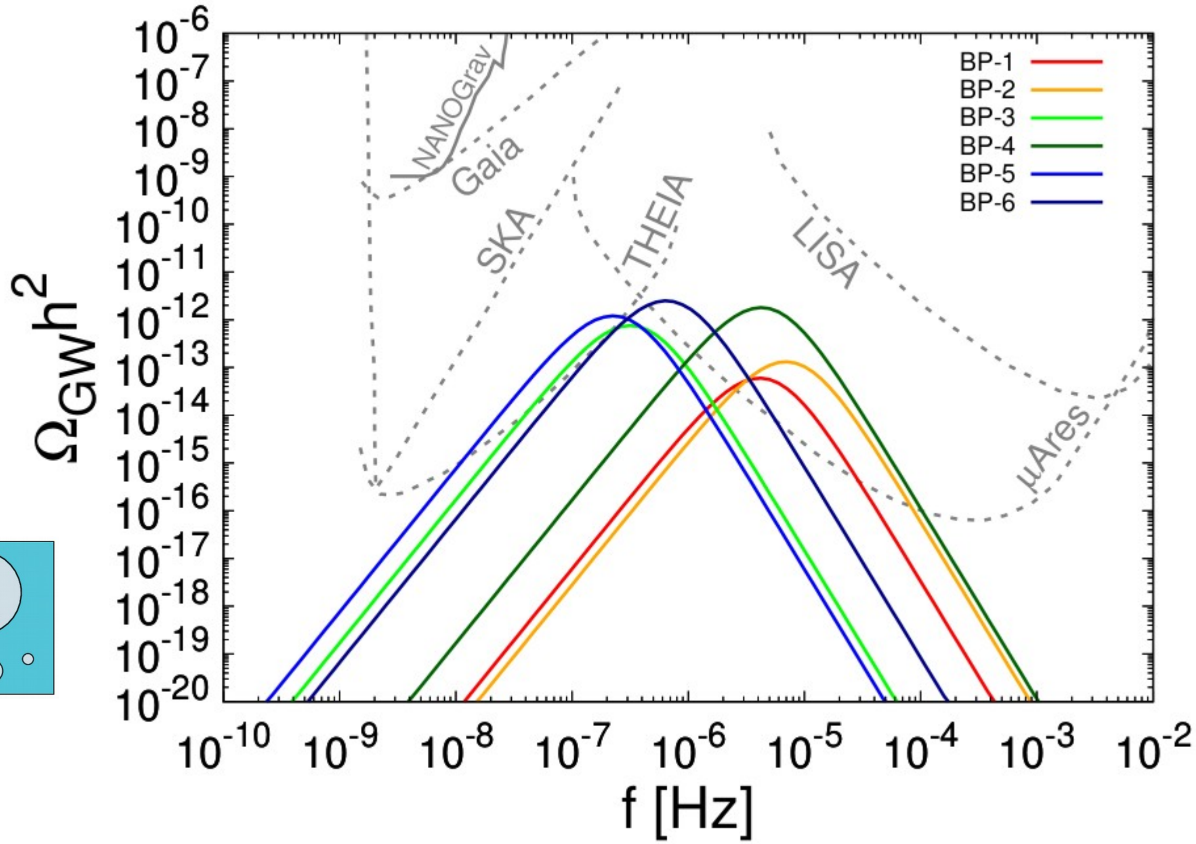

David J. Weir: Higgs physics and cosmology: gravitational waves from the electroweak phase transition

PBHs and Pulsar Timing Array: Tristram Acuna’s talk

Summary

Summary

- We discussed several detectable signals of PBHs with different mass.
- 511keV gamma-ray line excess can be interpreted by PBH $1.0 \times 10^{-17} \lesssim M_{\rm PBH}/M_\odot \lesssim 8.0 \times 10^{-17}$ via Hawking radiation
- SN Ia event rate associates with PBHs $7.6 \times 10^{-13} \leq M_{\rm PBH}/M_\odot \leq 6.1 \times 10^{-12}$, transiting through WDs.
- Introduce a dark sector model, which efficiently produces sub-solar-mass PBHs through FOPT and associates to the boosted DM.

Thank you for your attention!

Back up

Discussion: FB stability

- The stable conditions for FBs not decay to χ or fission to lighter FBs

$$\frac{dM_{\rm FB}}{dQ_{\rm FB}} < m + g_\chi v_\phi, \quad \text{and} \quad \frac{d^2 M_{\rm FB}}{dQ_{\rm FB}^2} < 0$$

- χ-e scattering, the χ may be ejected from FB unless its mean free path is short enough that multiple scattering with other χ in the FB slows it down.

- The χ-χ scattering $\sigma_{\chi\chi}$ via ϕ is larger than $\sigma_{\chi e} < 10^{-31}\ {\rm cm}^2$. The $\ell_\chi \equiv (n_\chi \sigma_{\chi\chi})^{-1}$ is much smaller than $R_{\rm FB}$.

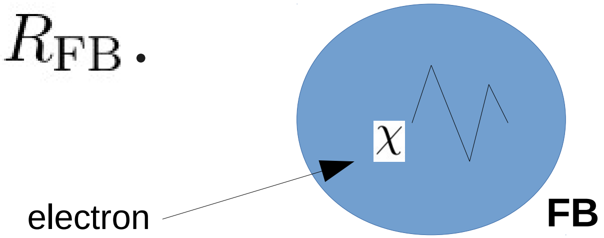

Discussion: relic of dark scalar

- During FB formation, ϕ can be copiously produced via $\chi\bar{\chi} \to \phi\phi$
Since ϕ is non-relativistic and evolve like matter, so that its relic density may overclose the Universe.

- To avoid this, we allow ϕ decay to a pair of relativistic scalars s, which preserves the relativistic degree of freedom in dark sector. We require $\Delta N_{\rm eff} \leq 0.5$.

- The trilinear term $\mu\phi s s$

$$\tau_{\phi\to ss} \simeq 6.6 \times 10^{-20} \left(\frac{\rm MeV}{\mu}\right)^2 \left(\frac{m_\phi}{\rm MeV}\right) \; [\rm sec]$$

PBH and Pulsar Timing Array

PBH: Pulsar Timing Array

- The millisecond pulsars provide accurate timing signals, and are exploited to measure the gravitational waves (GW).
- The NANOGrav collaboration observed 67 pulsars for 15 yr and reported the correlations of Helling-Downs pattern, pointing to the stochastic GW.

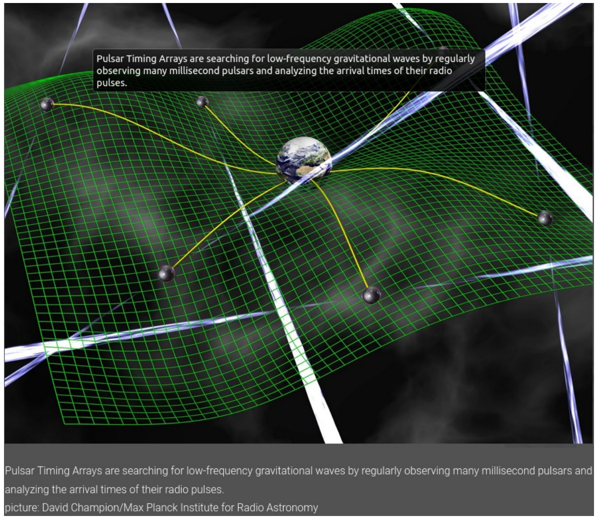

Pulsar Timing Arrays | Max Planck Institute for Gravitational Physics (Albert Einstein Institute)

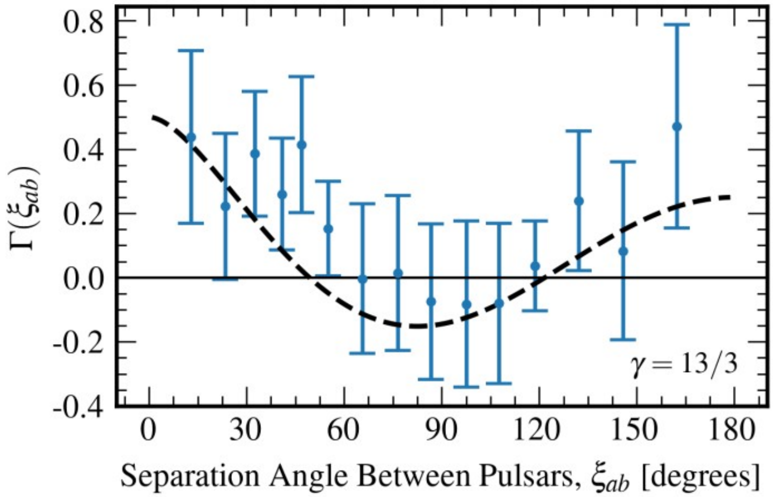

Helling-Downs pattern from NANOGrav 15 yr, arXiv:2306.16213

PBH: Pulsar Timing Array

- Pulsar timing as probe of PBHs. J.T.Acuna,P.Y.Tseng, arXiv:2306.16213
- Pulsar signals arriving on Earth can be characterized by its phase

$$\boxed{\phi(t) = \phi_0 + \underbrace{\nu}_{\text{frequency}} t + \underbrace{\frac{\dot{\nu}}{2}}_{\text{Spin-down}} t^2}$$

- Third-order from transiting PBHs: i) in the vicinity of the pulsar induce-->*Doppler phase shift*, ii) close to the Earth-pulsar line of sight-->*Shapiro time delay*.

Doppler: $$\left(\frac{\delta\nu}{\nu}\right)_D = \frac{1}{c}\int dt\ \hat{d}\cdot\vec{\nabla}\Phi,$$

Shapiro: $$\left(\frac{\delta\nu}{\nu}\right)_S = -\frac{2}{c^3}\int_{LOS} dz\ \vec{v}\cdot\vec{\nabla}\Phi,$$

PBH gravitational potential

PBH: Pulsar Timing Array

- The corresponding phase shift is

$$\boxed{\delta\phi(t) = \int^t dt' \; \delta\nu(t')}$$

- The residual signal amplitude after subtracting the phase shift from the 1st and the 2nd order

$$h_I(t) = \sum_{i=1}^{N} \delta\phi_{I,i}(t) - \delta\phi_{0,I}(t), \quad \delta\phi_{0,I} \equiv \sum_{n=0}^{2} f_n(t) \left[\frac{1}{T_{obs}} \int_0^{T_{obs}} dt' \; \sum_{i=1}^{N} \delta\phi_{I,i}(t') f_n(t') \right]$$

- The signal-to-noise ratio is given as

$$\boxed{\mathrm{SNR}_I^2 = \frac{1}{\nu_I^2 t_{rms}^2 \Delta t} \int_0^{T_{obs}} dt \; h_I^2(t)}$$

J.T.Acuna,P.Y.Tseng, arXiv:2306.16213

PBH: Pulsar Timing Array

- The projecting sensitivity of SKA, assuming 20 yr observation of 200 pulsars with 50 ns uncertainty in the pulsar timing data and 2 weeks cadence:

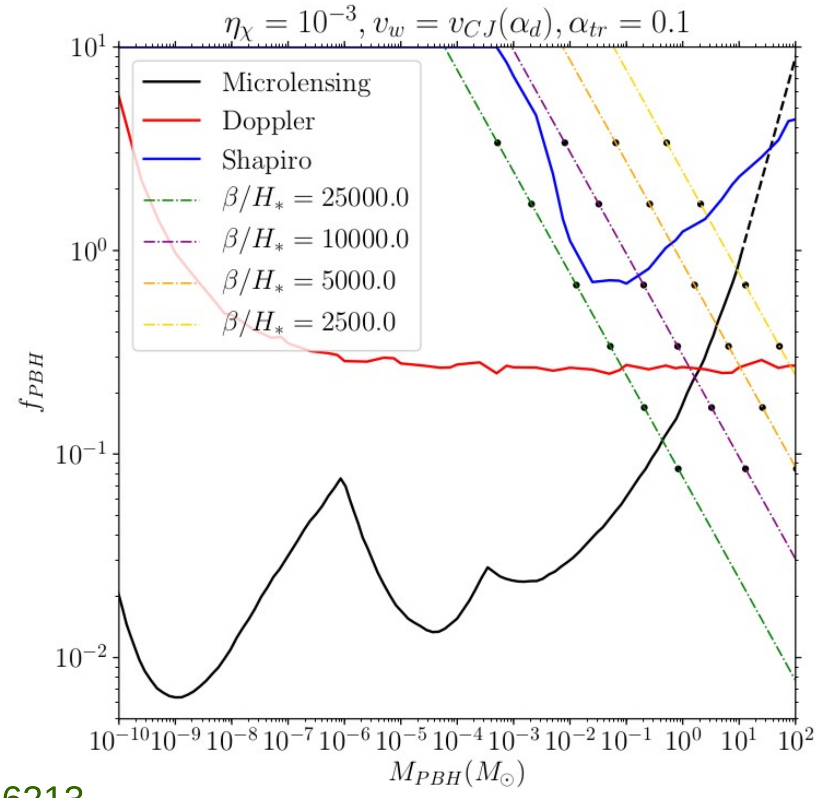

J.T.Acuna,P.Y.Tseng, arXiv:2306.16213

PBH formation:

FOPT→FB→PBH

Trapping DM

- During FOPT, lighter (heavier) χ locate outside (inside) the bubble, and momentum conservation much be satisfied at the bubble wall.

Outside

$\langle\phi\rangle = 0,\ m_\chi = m$

Inside

$\langle\phi\rangle \neq 0,\ m_\chi = m + g_\chi v_\phi$

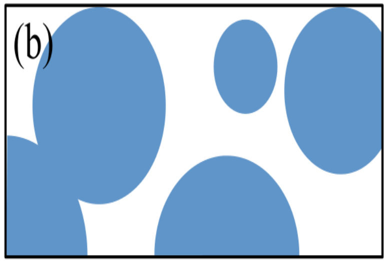

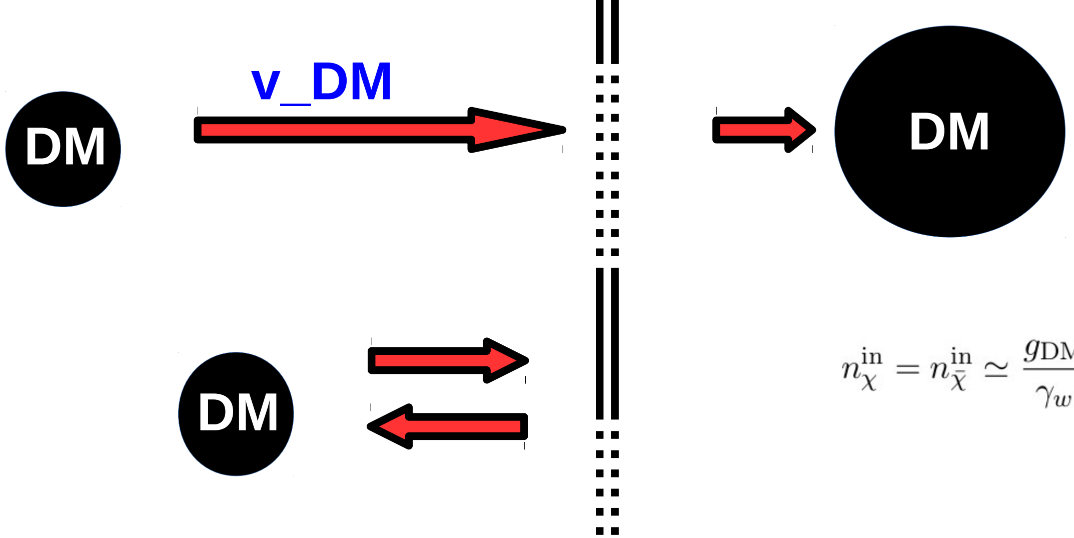

$$n_\chi^{\rm in} = n_{\bar\chi}^{\rm in} \simeq \frac{g_{\rm DM} T_\star^3}{\gamma_w v_w}\left(\frac{\gamma_w(1-v_w)m_\chi/T_\star + 1}{4\pi^2\gamma_\omega^3(1-v_w)^2}\right) e^{-\frac{\gamma_w(1-v_w)m_\chi}{T_\star}}$$

Bubble Wall v_w

FB formation

- Suppose χ particle mass difference is large: $\Delta m_\chi \simeq g_\chi v_\phi > T_c$
- χ particles, remaining in **outside** the bubble (trapped in the *false vacuum*), will be aggregated by the expanding bubbles and form a macroscopic **Fermi-Ball(FB)**.
- For this to occur, there must be non-zero **asymmetry** $\eta_\chi \equiv (n_\chi - n_{\bar{\chi}})/s$ in the false vacuum so that the an excess remain after pair annihilation.
- **FB** stability: $\boxed{\dfrac{dM_{\rm FB}}{dQ_{\rm FB}} < m + g_\chi v_\phi, \quad \text{and} \quad \dfrac{d^2 M_{\rm FB}}{dQ_{\rm FB}^2} < 0}$

Signals from FB

Gravitational wave from FOPT

- The associated gravitational wave signals from FOPT:

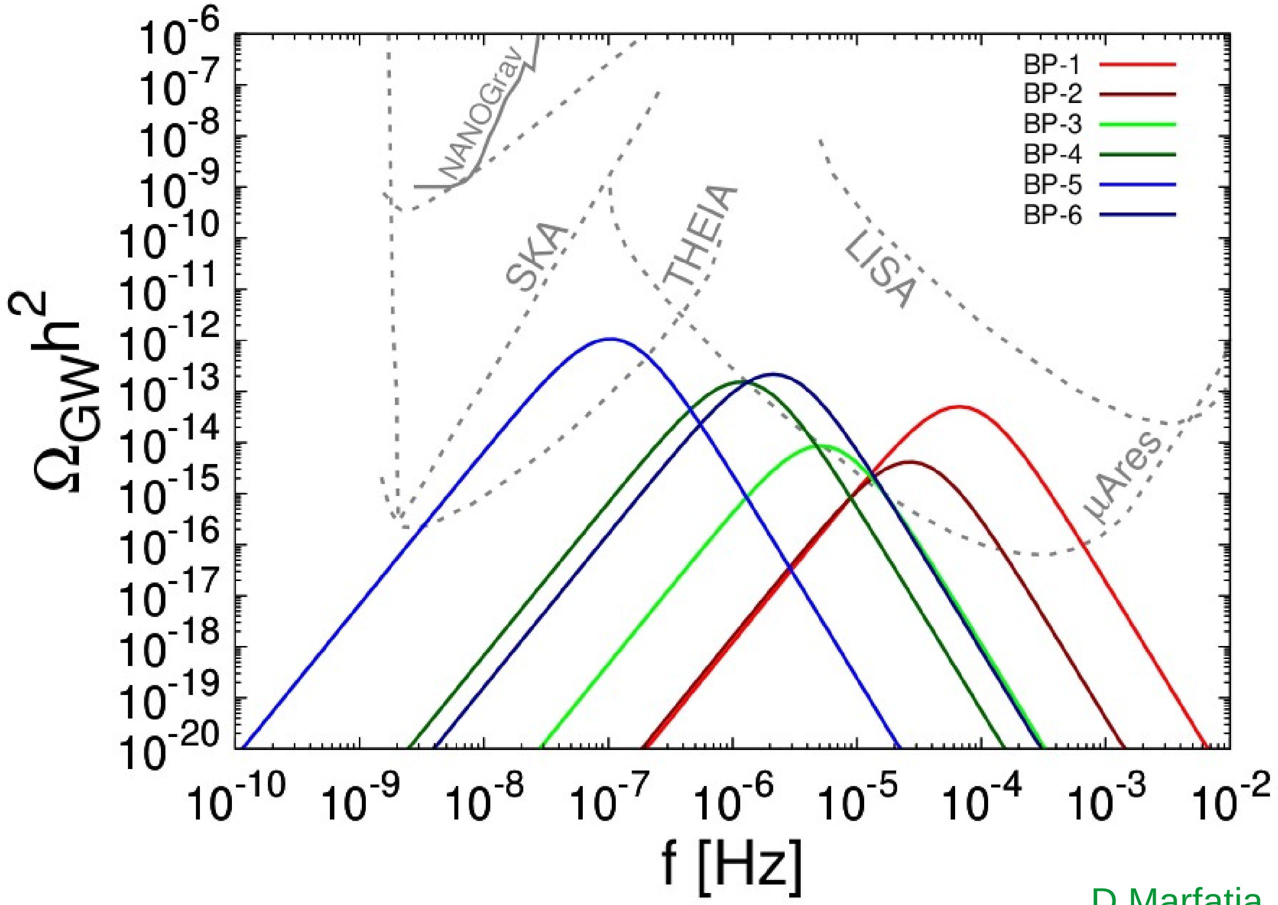

D.Marfatia, P.Y. Tseng: 2107.00859

Fermi ball

- We consider the finite-temperature quartic effective potential:

D.Marfatia, P.Y. Tseng: 2107.00859

Table 1. Benchmark points with $A = 0.1$. $N_{\rm events}$ is the number of microlensing events expected in 70 hours of observation of M31 by Subaru-HSC.

	BP-1	BP-2	BP-3	BP-4	BP-5	BP-6	BP-7	BP-8
λ	0.134	0.158	0.193	0.078	0.062	0.072	0.053	0.060
$B^{1/4}$/keV	2.42	43.5	34.9	64.2	63.6	73.2	284	1390
C/keV	0.059	6.234	4.988	3.080	0.315	0.586	0.342	7.713
D	5.807	0.451	0.720	0.445	0.257	0.293	0.584	0.706
η_χ	7.34×10^{-6}	1.37×10^{-7}	3.51×10^{-6}	4.55×10^{-8}	6.98×10^{-9}	3.64×10^{-9}	8.54×10^{-9}	2.40×10^{-8}
$T_{{\rm SM}\star}$/keV	1.41	100.0	64.5	128.1	164.8	169.5	427.8	1601
$T_\star$/keV	0.57	34.2	21.6	52.3	84.8	86.9	201.0	879.0
T_f/keV	0.63	41.4	25.9	64.4	92.9	92.5	233.2	1005
$S_3(T_\star)/T_\star$	189	188	187	186	187	184	177	171
$M_{\rm FB}/M_\odot$	3.37×10^{-6}	1.11×10^{-6}	9.66×10^{-6}	1.01×10^{-7}	1.08×10^{-8}	1.08×10^{-9}	9.66×10^{-11}	1.09×10^{-11}
$R_{\rm FB}/R_\odot$	0.529	7.77×10^{-3}	2.15×10^{-2}	2.09×10^{-3}	1.00×10^{-3}	3.86×10^{-4}	2.83×10^{-5}	1.64×10^{-6}
$Q_{\rm FB}$	4.70×10^{56}	8.62×10^{54}	9.38×10^{55}	5.34×10^{53}	5.74×10^{52}	5.00×10^{51}	1.15×10^{50}	2.65×10^{48}
α	1.63×10^{-2}	1.56×10^{-2}	1.70×10^{-2}	2.83×10^{-2}	2.00×10^{-2}	1.24×10^{-2}	1.79×10^{-2}	2.62×10^{-2}
$\beta/H_\star$	3.43×10^4	1.57×10^3	3.01×10^3	2.04×10^3	1.86×10^3	2.80×10^3	4.44×10^3	5.59×10^3
$v_\phi/T_\star$	3.554	4.175	3.958	4.889	3.987	3.501	4.724	4.469
v_w	0.890	0.940	0.937	0.946	0.886	0.854	0.923	0.916
$\Omega_{\rm FB}h^2$	1.79×10^{-2}	5.81×10^{-3}	0.12	2.94×10^{-3}	4.56×10^{-4}	2.70×10^{-4}	2.39×10^{-3}	3.38×10^{-2}
$N_{\rm events}$	19.5	20.4	29.3	38.9	17.5	19.3	46.1	29.1
$\Delta N_{\rm eff}$	0.391	0.226	0.248	0.394	0.497	0.425	0.261	0.408

PBHs from FOPT

- The benchmark points for PBH formation from FOPT

Corresponding temperature of phase transition

	BP-1	BP-2	BP-3	BP-4	BP-5	BP-6
λ	0.097	0.177	0.084	0.198	0.198	0.077
$B^{1/4}/\mathrm{MeV}$	37.89	16.55	3.412	1.843	0.286	2.411
C/MeV	0.551	1.329	0.054	0.260	0.047	0.022
D	1.257	0.138	0.413	0.750	0.794	0.286
g_χ	0.031	0.020	0.187	0.240	0.118	0.164
η_χ	4.97×10^{-9}	4.67×10^{-11}	3.81×10^{-13}	9.40×10^{-16}	1.47×10^{-18}	9.26×10^{-17}
$T_{\mathrm{SM}\star}/\mathrm{MeV}$	29.81	53.46	7.821	2.939	0.440	4.979
$T_\star/\mathrm{MeV}$	18.72	36.89	3.156	1.126	0.157	2.908
T_f/MeV	19.73	37.13	3.338	1.343	0.214	3.071
T_ϕ/MeV	17.72	21.64	2.737	0.800	0.077	2.361
$S_3(T_\star)/T_\star$	156	161	165	170	180	170
$M_{\mathrm{PBH}}/M_\odot$	3.18×10^{-16}	1.08×10^{-16}	1.07×10^{-17}	1.07×10^{-18}	3.91×10^{-19}	3.99×10^{-20}
Q_{FB}	5.02×10^{42}	1.77×10^{42}	1.14×10^{42}	2.06×10^{41}	4.48×10^{41}	5.00×10^{39}
β'	3.83×10^{-17}	2.02×10^{-19}	8.01×10^{-23}	3.43×10^{-26}	5.45×10^{-30}	1.01×10^{-27}
α	1.26×10^{-2}	1.72×10^{-3}	2.78×10^{-3}	9.23×10^{-3}	1.81×10^{-2}	1.14×10^{-2}
$\beta/H_\star$	1.42×10^{4}	2.55×10^{3}	4.22×10^{3}	2.86×10^{3}	1.90×10^{3}	2.74×10^{3}
v_w	0.840	0.694	0.845	0.935	0.968	0.843
$\Omega_{\mathrm{PBH}}h^2$	0.108	9.74×10^{-4}	1.15×10^{-6}	1.57×10^{-9}	4.17×10^{-13}	2.52×10^{-10}
ΔN_{eff}	0.413	0.406	0.087	0.114	0.165	0.379

D.Marfatia, P.Y. Tseng: 2107.00859

Microlensing

- These FB mass and radius ranges can induce microlensing effects.

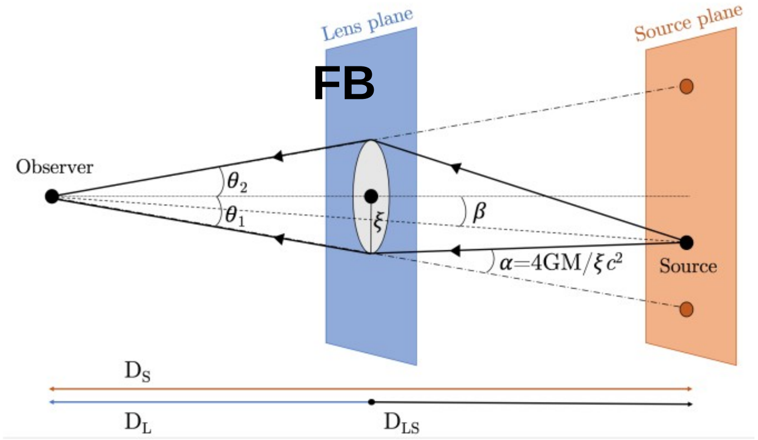

$$\theta_E \equiv \sqrt{\frac{4GM}{c^2}\frac{D_{LS}}{D_L D_S}}$$

$$\mu_{\rm tot} = \frac{u^2+2}{u\sqrt{u^2+4}} \xrightarrow{u=1} 1.34 \, .$$

D.Croon, D. McKeen, N. Raj: 2002.08962

- The separating angle of two images of the background star are too small to be resolved, but we can observe the sudden luminosity enhancement of the star.

Microlensing

- Astrophysical Sky surveys are ideal for observing microlensing. Ex. Subaru-HSC (observing M31 for 7 hrs).

FB halos surround MW and M31. FBs and stars have relative velocity of 250 km/s.

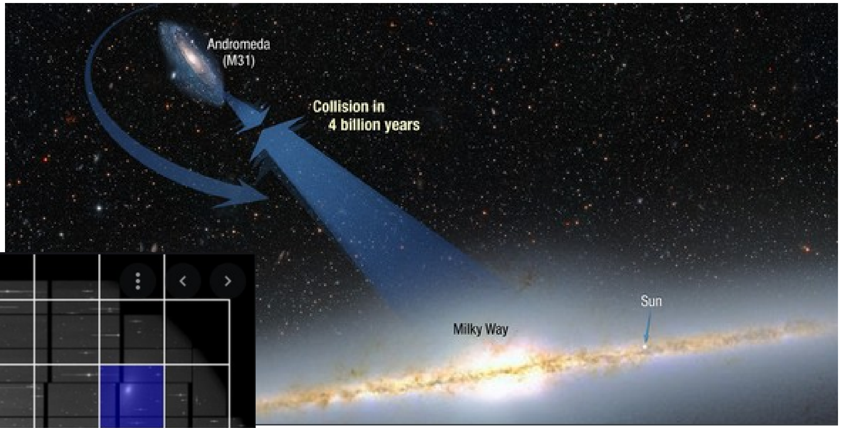

Milky Way Destined for Head-On Collision | NASA

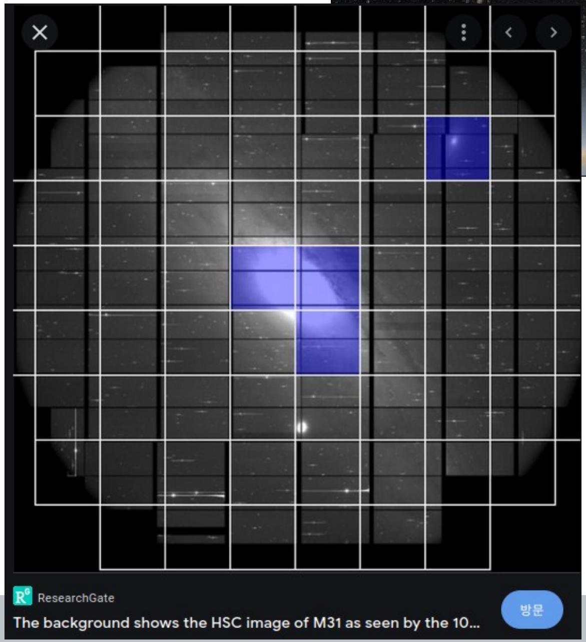

M31 image from Subaru-HSC

Relativistic degree of freedom

- The temperature of FOPT is lower than the BBN, and robust 95% CL upper limit is $\Delta N_{\rm eff} \lesssim 0.5$. 2009.09745, 1103.1261

Table 1. Benchmark points with $A = 0.1$. $N_{\rm events}$ is the number of microlensing events expected in 70 hours of observation of M31 by Subaru-HSC.

	BP-1	BP-2	BP-3	BP-4	BP-5	BP-6	BP-7	BP-8
λ	0.134	0.158	0.193	0.078	0.062	0.072	0.053	0.060
$B^{1/4}$/keV	2.42	43.5	34.9	64.2	63.6	73.2	284	1390
C/keV	0.059	6.234	4.988	3.080	0.315	0.586	0.342	7.713
D	5.807	0.451	0.720	0.445	0.257	0.293	0.584	0.706
η_χ	7.34×10^{-6}	1.37×10^{-7}	3.51×10^{-6}	4.55×10^{-8}	6.98×10^{-9}	3.64×10^{-9}	8.54×10^{-9}	2.40×10^{-8}
$T_{\rm SM\star}$/keV	1.41	100.0	64.5	128.1	164.8	169.5	427.8	1601
$T_\star$/keV	0.57	34.2	21.6	52.3	84.8	86.9	201.0	879.0
T_f/keV	0.63	41.4	25.9	64.4	92.9	92.5	233.2	1005
$S_3(T_\star)/T_\star$	189	188	187	186	187	184	177	171
$M_{\rm FB}/M_\odot$	3.37×10^{-6}	1.11×10^{-6}	9.66×10^{-6}	1.01×10^{-7}	1.08×10^{-8}	1.08×10^{-9}	9.66×10^{-11}	1.09×10^{-11}
$R_{\rm FB}/R_\odot$	0.529	7.77×10^{-3}	2.15×10^{-2}	2.09×10^{-3}	1.00×10^{-3}	3.86×10^{-4}	2.83×10^{-5}	1.64×10^{-6}
$Q_{\rm FB}$	4.70×10^{56}	8.62×10^{54}	9.38×10^{55}	5.34×10^{53}	5.74×10^{52}	5.00×10^{51}	1.15×10^{50}	2.65×10^{48}
α	1.63×10^{-2}	1.56×10^{-2}	1.70×10^{-2}	2.83×10^{-2}	2.00×10^{-2}	1.24×10^{-2}	1.79×10^{-2}	2.62×10^{-2}
$\beta/H_\star$	3.43×10^4	1.57×10^3	3.01×10^3	2.04×10^3	1.86×10^3	2.80×10^3	4.44×10^3	5.59×10^3
$v_\phi/T_\star$	3.554	4.175	3.958	4.889	3.987	3.501	4.724	4.469
v_w	0.890	0.940	0.937	0.946	0.886	0.854	0.923	0.916
$\Omega_{\rm FB}h^2$	1.79×10^{-2}	5.81×10^{-3}	0.12	2.94×10^{-3}	4.56×10^{-4}	2.70×10^{-4}	2.39×10^{-3}	3.38×10^{-2}
$N_{\rm events}$	19.5	20.4	29.3	38.9	17.5	19.3	46.1	29.1
$\Delta N_{\rm eff}$	0.391	0.226	0.248	0.394	0.497	0.425	0.261	0.408

Temperature of FOPT

Gravitational Wave

Gravitational wave production

- A FOPT generates GWs from three processes: I). Bubble collisions, II). Sound wave in the plasma, III) Magnetohydrodynamic (MHD) turbulence.

- The relevant parameters are required to calculate the GW signals:

$$
\begin{cases}
T_\star\,, \\
\alpha \equiv \dfrac{\left(1-T\frac{\partial}{\partial T}\right)\Delta V_{\rm eff}|_{T_\star}}{\rho(T_\star)}\,, \quad \rho \equiv \pi^2 g_\star T^4/30 \\
\dfrac{\beta}{H_\star} \simeq T_\star \dfrac{d(S_3/T)}{dT}\Big|_{T_\star} \\
v_w
\end{cases}
$$

Gravitational wave production

- A FOPT generates GWs from three processes: I). Bubble collisions, II). Sound wave in the plasma, III) Magnetohydrodynamic (MHD) turbulence.

- The Euclidean action:

$$\boxed{S_3(T) = 4\pi \int_0^\infty r^2 dr \left[\frac{1}{2} \left(\frac{d\phi}{dr} \right)^2 + V_{\rm eff}(\phi, T) \right]}$$

- Bubble nucleation rate per unit volume:

$$\boxed{\Gamma(T) = T^4 \left(\frac{S_3}{2\pi T} \right)^{3/2} e^{-\frac{S_3}{T}}}$$

Gravitational wave production

- A FOPT generates GWs from three processes: I). Bubble collisions, II). Sound wave in the plasma, III) Magnetohydrodynamic (MHD) turbulence.

- The fraction of space in the false vacuum:

$$\boxed{F(t) = \exp\left[-\frac{4\pi}{3} v_w^3 \int_{t_c}^{t} dt' (t - t')^3 \Gamma(t')\right]}$$

- The percolation temperature $T_\star$ of FOPT is determined by :

$$\boxed{F(t_\star) = 1/e \simeq 0.37}$$

Gravitational wave production

- A FOPT generates GWs from: I). Bubble collisions

$$h^2\Omega_{\rm env}(f) \;=\; 1.67\times 10^{-5}\left(\frac{H_*}{\beta}\right)^2\left(\frac{\kappa\alpha}{1+\alpha}\right)^2\left(\frac{100}{g_*}\right)^{\frac{1}{3}}\left(\frac{0.11\,v_w^3}{0.42+v_w^2}\right)S_{\rm env}(f)$$

C.Caprini et. al: 1512.06239

$$S_{\rm env}(f)=\frac{3.8\,(f/f_{\rm env})^{2.8}}{1+2.8\,(f/f_{\rm env})^{3.8}}$$

- The peak frequency is determined by the time scale of FOPT $1/\beta$:

$$\frac{f_*}{\beta}=\left(\frac{0.62}{1.8-0.1v_w+v_w^2}\right)$$

Gravitational wave production

- A FOPT generates GWs from: I). Bubble collisions

$$h^2\Omega_{\rm env}(f) \;=\; 1.67\times10^{-5}\left(\frac{H_*}{\beta}\right)^2\left(\frac{\kappa\alpha}{1+\alpha}\right)^2\left(\frac{100}{g_*}\right)^{\frac{1}{3}}\left(\frac{0.11\,v_w^3}{0.42+v_w^2}\right)\,S_{\rm env}(f)$$

C.Caprini et. al: 1512.06239

$$S_{\rm env}(f) = \frac{3.8\,(f/f_{\rm env})^{2.8}}{1+2.8\,(f/f_{\rm env})^{3.8}}$$

- The peak frequency is determined by the time scale of FOPT. Then red-shift to present epoch

$$f_{\rm env} = 16.5\times10^{-3}\,{\rm mHz}\left(\frac{f_*}{\beta}\right)\left(\frac{\beta}{H_*}\right)\left(\frac{T_*}{100\,{\rm GeV}}\right)\left(\frac{g_*}{100}\right)^{\frac{1}{6}}$$

Gravitational Wave

- GW spectra from the benchmark points:

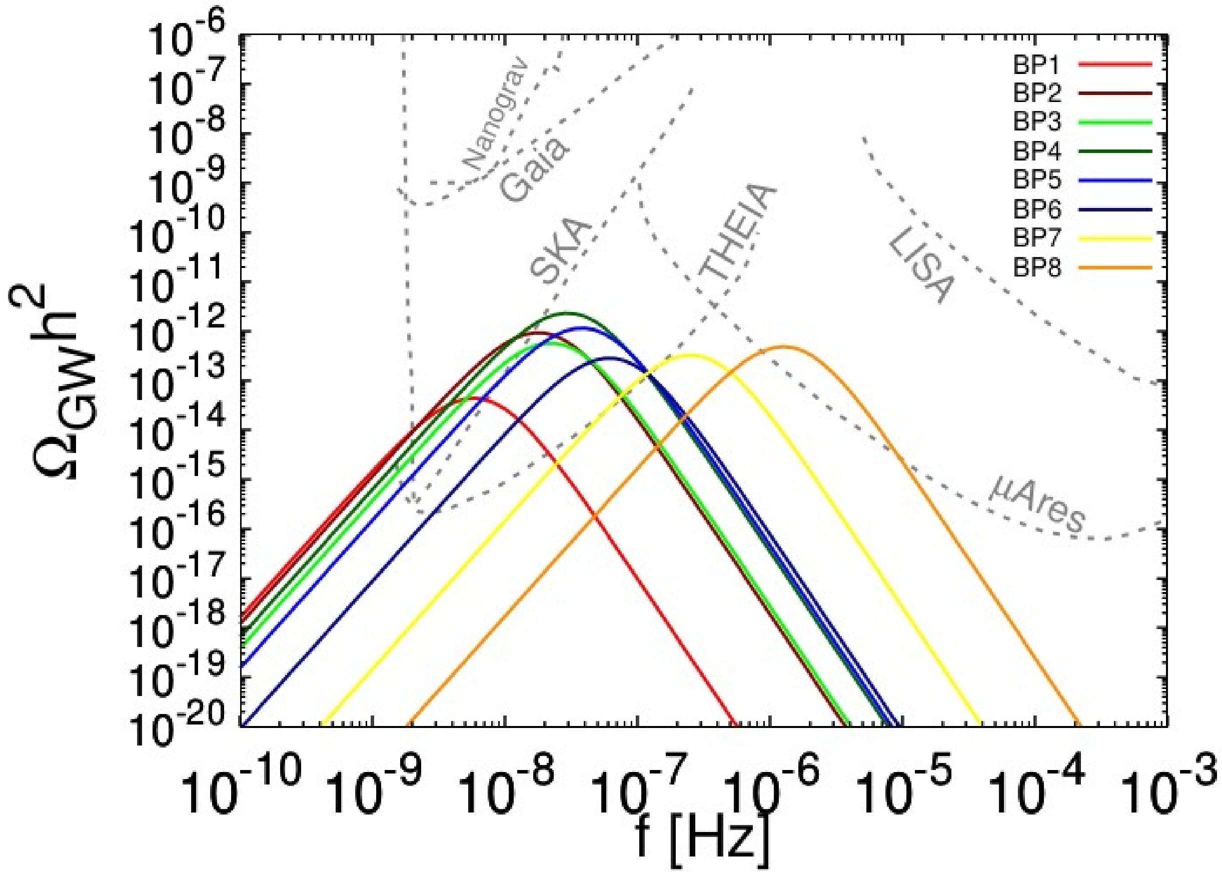

D.Marfatia, P.Y. Tseng: 2107.00859

PBH: benchmark points

- Benchmark points for PBHs from FOPT.

D.Marfatia, P.Y. Tseng:2112.14588

	BP-1	BP-2	BP-3	BP-4	BP-5	BP-6
λ	0.061	0.110	0.195	0.087	0.150	0.158
$B^{1/4}$/MeV	75.14	13.81	1.501	1.261	0.121	2.999
C/MeV	0.249	0.462	0.078	0.052	0.011	0.325
D	0.596	1.458	1.119	0.596	1.418	0.519
g_χ	1.088	1.301	1.011	1.289	0.983	1.228
η_χ	1.03×10^{-9}	1.28×10^{-10}	1.64×10^{-12}	1.21×10^{-15}	2.59×10^{-18}	6.26×10^{-17}
m/MeV	53.41	0.120	0.259	0.394	0.341	1.704
$T_{\rm SM\star}$/MeV	94.68	14.63	0.895	2.104	0.164	4.774
$T_\star$/MeV	53.16	6.143	0.421	0.868	0.052	2.287
T_f/MeV	59.63	6.888	0.472	1.023	0.068	2.571
T_ϕ/MeV	53.09	6.045	0.415	0.857	0.050	1.950
$S_3(T_\star)/T_\star$	155	159	166	171	180	170
$M_{\rm PBH}/M_\odot$	2.92×10^{-16}	1.15×10^{-16}	1.19×10^{-17}	1.93×10^{-18}	3.91×10^{-19}	4.23×10^{-20}
$Q_{\rm FB}$	1.26×10^{42}	4.31×10^{42}	5.96×10^{42}	5.01×10^{41}	7.58×10^{41}	4.18×10^{39}
β'	2.80×10^{-17}	2.54×10^{-19}	7.78×10^{-23}	4.45×10^{-26}	5.75×10^{-30}	8.97×10^{-28}
α	1.48×10^{-2}	7.40×10^{-3}	1.20×10^{-2}	1.12×10^{-2}	1.35×10^{-2}	1.30×10^{-2}
$\beta/H_\star$	4.41×10^{3}	9.36×10^{3}	3.21×10^{4}	3.25×10^{3}	4.94×10^{3}	2.64×10^{3}
v_w	0.904	0.904	0.904	0.930	0.963	0.905
v_ϕ/MeV	224	23.1	1.426	3.821	0.247	8.157
$dM_{\rm FB}/dQ_{\rm FB}$/MeV	258	28.3	1.980	4.264	0.573	10.89
$\Omega_{\rm PBH}h^2$	0.079	1.12×10^{-3}	1.09×10^{-6}	1.52×10^{-9}	2.15×10^{-13}	6.35×10^{-29}
$\Delta N_{\rm eff}$	0.218	0.126	0.208	0.146	0.147	0.221

Gravitational Wave

- GW spectra from the benchmark points:

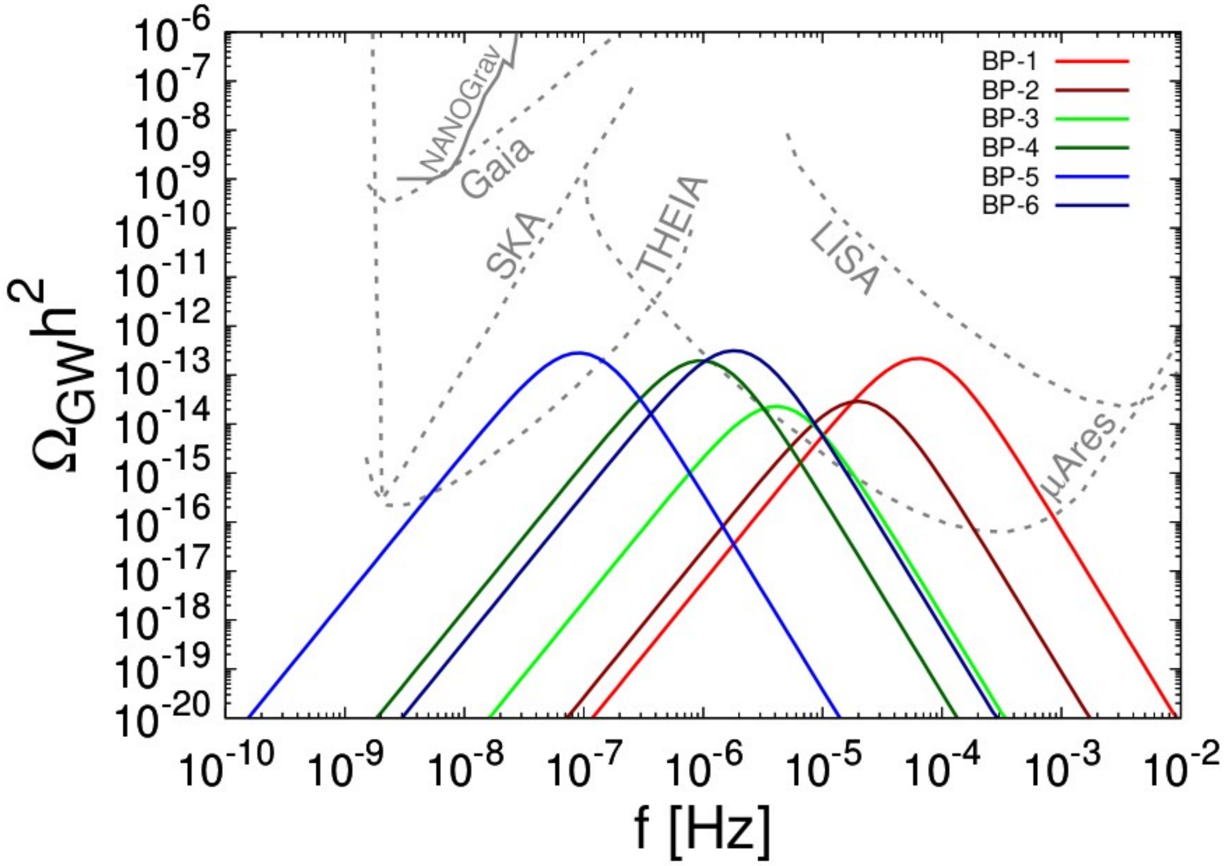

D.Marfatia, P.Y. Tseng: 2112.14588

PBH evaporation

- The evaporation of a PBH produces all particles with mass below the PBH temperature:

Kazunori Kohri et.al: 2002.12778

$$T_{\rm PBH} \simeq 5.3 \text{ MeV} \times \left(\frac{10^{-18} M_\odot}{M_{\rm PBH}}\right)$$

- For $M_{\rm PBH}/M_\odot \lesssim 2 \times 10^{-19}$, PBHs evaporated before today.

- The Hawking emission rate of primary particles:

$$\frac{dN_i}{dEdt} = \frac{n_i^{\rm d.o.f} \Gamma_i(E, M_{\rm PBH})}{2\pi(e^{E/T_{\rm PBH}} \pm 1)}$$

A.Arbey, J.Auffinger (BlackHawk): 1905.04268

PBH evaporation

- The extragalactic gamma-ray background due to PBH evaporation

Kazunori Kohri et.al: 2002.12778

$$\boxed{\frac{d^2\Phi}{dEdt} = \int_{t_{\rm CMB}}^{\min(t_{\rm eva},t_0)} c[1+z(t)]\frac{f_{\rm PBH}\rho_{\rm DM}}{M_{\rm PBH}}\frac{d^2N_\gamma}{d\tilde{E}dt}\bigg|_{\tilde{E}=[1+z(t)]E} dt}$$

with average DM density $\rho_{\rm DM} = 1.27\ {\rm GeV\,m^{-3}}$.

- The evolution of the Universe is approximated as matter dominated until the current epoch

$$1 + z(t) = \left(\frac{t_0}{t}\right)^{2/3}$$

Correlated GW and gamma-ray signals

- β' is defined at PBH formation as:

Kazunori Kohri et.al: 2002.12778

$$\boxed{\beta' \equiv \gamma^{1/2} \left(\frac{g_*(T_\phi)}{106.75}\right)^{-1/4} \left(\frac{h}{0.67}\right)^{-2} \frac{\rho_{\rm PBH}(T_\phi)}{\rho(T_\phi)}}$$

- γ is the ratio between BH mass to the horizon mass in radiation dominated era. In our scenario, it gives

$$\boxed{\gamma^{1/2} \left(\frac{g_*(T_\phi)}{106.75}\right)^{-1/4} = 4.58 \times 10^{-12} \frac{T_\phi}{\rm MeV} \left(\frac{M_{\rm PBH}}{10^{-18} M_\odot}\right)^{1/2}}$$

Part-1: Bubble wall velocity

- Particles reflected by the bubble wall exert pressure on it, and slow down the bubble wall velocity.

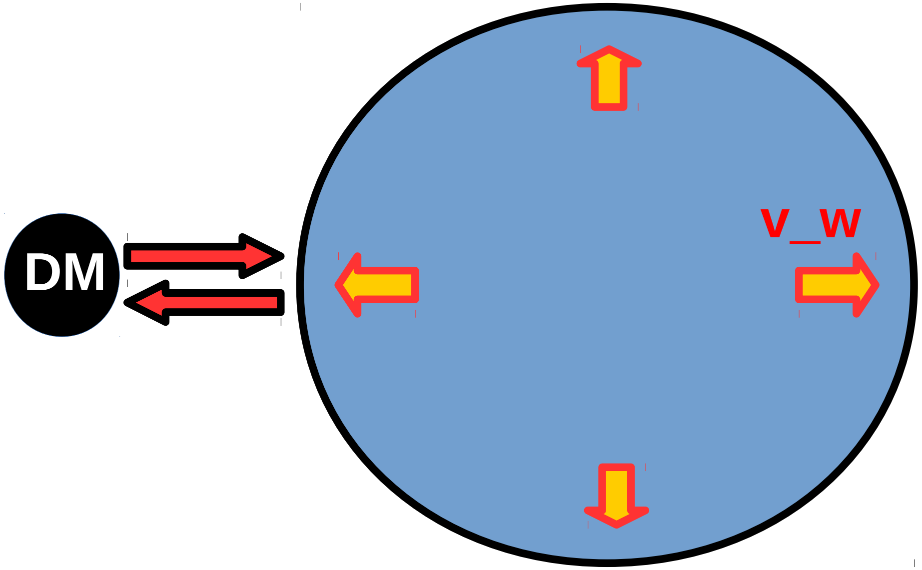

Part-1: Bubble filtering

- If a thermal DM flux is incident on the wall, the number density of DM that enter the bubble is:

$$\boxed{n_\chi^{\rm in} = n_{\bar\chi}^{\rm in} \simeq \frac{g_{\rm DM} T_\star^3}{\gamma_w v_w} \left(\frac{\gamma_w (1-v_w) m_\chi / T_\star + 1}{4\pi^2 \gamma_\omega^3 (1-v_w)^2} \right) e^{-\frac{\gamma_w (1-v_w) m_\chi}{T_\star}}}$$

D.Chway, T.H.Jung, C.S.Shin: 1912.04238

- DMs are filtered by the non-relativistic and relativistic bubble wall velocity:

$$\boxed{n_\chi^{\rm in} = \begin{cases} \sim e^{-m_\chi/T_\star} & \text{for} \quad v_w \to 0 \\ \sim e^{-m_\chi/(2\gamma_w T_\star)} & \text{for} \quad m_\chi/(\gamma_w T_\star) \to 0 \end{cases}}$$

Part-1: Bubble filtering

- If $T_\star < T_{\rm dec}$, the DM inside the bubble is decoupled from the thermal bath and become DM relic abundance.

- DM relic abundance today can be calculated by dividing $n_\chi^{\rm in}+n_{\bar\chi}^{\rm in}$ by entropy $s = (2\pi^2/45) g_{\star S} T^3$:

$$\boxed{\Omega_{\rm DM}h^2 \simeq 6.29\times 10^8\, \frac{m_\chi (n_\chi^{\rm in}+n_{\bar\chi}^{\rm in})}{\rm GeV}\, \frac{1}{g_{\star S} T_\star^3}}$$

$$\boxed{\Omega_{\rm DM}h^2 \simeq \begin{cases} 1.27\times 10^8 \left(\frac{m_\chi}{\rm GeV}\right)\left(\frac{g_{\rm DM}}{g_{\star S}}\right)\left(\frac{m_\chi}{2\gamma_w T_\star}+1\right) e^{-\frac{m_\chi}{2\gamma_w T_\star}}\,, & \text{for } v_w \to 1 \\ 3.19\times 10^7 \left(\frac{m_\chi}{\rm GeV}\right)\left(\frac{g_{\rm DM}}{g_{\star S}}\right)\left(\frac{1}{v_w}\right)\left(\frac{m_\chi}{T_\star}+1\right) e^{-\frac{m_\chi}{T_\star}}\,, & \text{for } v_w \to 0. \end{cases}}$$

Part-1: Bubble wall velocity

- In the ultrarelativistic limit, the pressure on bubble wall can be obtain from the light degree of freedom inside and outside the bubble:

D.Chway et.al : 1912.04238
J.R.Espinosa et.al: 1004.4187
D.Bodeker et.al : 0903.4099

$$\boxed{P = \frac{d_n g_\star \pi^2}{90}(1+v_w)^3\gamma_\omega^2 T_\star^4}$$

$$\boxed{d_n \equiv \frac{1}{g_\star}\left[\sum_{0.2M_i>\gamma_w T_\star}\left(g_i^b + \frac{7}{8}g_i^f\right)\right]}$$

- The v_w can be obtained by solving the eq. $P = \Delta V_{\text{eff}}$:

$$\boxed{\alpha = \frac{d_n}{3}(1+v_w)^3\gamma_\omega^2}$$

$$\boxed{\alpha \equiv \frac{\left(1-T\frac{\partial}{\partial T}\right)\Delta V_{\text{eff}}|_{T_\star}}{\rho(T_\star)}, \quad \rho \equiv \pi^2 g_\star T^4/30}$$

Part-1: Bubble wall velocity

- For bubble wall velocity v_w faster than the sound speed in plasma, but not ultrarelativistic, we use the approximation:

P.J.Steinhardt, Phys. Rev. D. 25, 2074 (1982)

$$\boxed{v_w = \frac{\frac{1}{\sqrt{3}} + \sqrt{\alpha^2 + \frac{2}{3}\alpha}}{1+\alpha}}$$

Part-2: anti-correlation

- The percolation condition using saddle point approximation:

$$\boxed{F(t) = \exp\left[-\frac{4\pi}{3} v_w^3 \int_{t_c}^{t} dt' (t-t')^3 \Gamma(t')\right]} \qquad \boxed{F(t_\star) = 1/e \simeq 0.37}$$

$$\boxed{8\pi v_w^3 \Gamma(T_\star) \beta^{-4} \simeq 1}$$

- Since $\beta/H_\star$ is almost constant, thus $\beta \propto H_\star \propto T_\star^2$ and from above condition, we have

$$\boxed{T_\star^{-4}\, e^{-S_3(T_\star)/T_\star} \simeq B^{-1}\, e^{-S_3(T_\star)/T_\star} \simeq \text{constant}\,, \quad \text{i.e.,} \quad e^{-S_3(T_\star)/T_\star} \propto B}$$

- Bubble nucleation rate per unit volume grow with vacuum energy density.

- For fixed $\Omega_{\rm FB} h^2$, we obtain $\boxed{M_{\rm FB} \propto 1/n_{\rm FB}|_{T_0} \propto e^{3/4\cdot(S_3(T_\star)/T_\star)} \propto B^{-3/4}}$